




# RGS3L allows for an M<sub>2</sub> muscarinic receptor-mediated RhoA-dependent inotropy in cardiomyocytes

Magdolna K. Levay<sup>1,7</sup> · Kurt A. Krobert<sup>2</sup> · Andreas Vogt<sup>1</sup> · Atif Ahmad<sup>1</sup> · Andreas Jungmann<sup>3</sup> · Christiane Neuber<sup>4</sup> · Sebastian Pasch<sup>5,7</sup> · Arne Hansen<sup>4,7</sup> · Oliver J. Müller<sup>6,7</sup> · Susanne Lutz<sup>5,7</sup> · Thomas Wieland<sup>1,7</sup> 

Received: 18 January 2021 / Revised: 27 January 2022 / Accepted: 28 January 2022  
© The Author(s) 2022

## Abstract

The role and outcome of the muscarinic M<sub>2</sub> acetylcholine receptor (M<sub>2</sub>R) signaling in healthy and diseased cardiomyocytes is still a matter of debate. Here, we report that the long isoform of the regulator of G protein signaling 3 (RGS3L) functions as a switch in the muscarinic signaling, most likely of the M<sub>2</sub>R, in primary cardiomyocytes. High levels of RGS3L, as found in heart failure, redirect the G<sub>i</sub>-mediated Rac1 activation into a G<sub>i</sub>-mediated RhoA/ROCK activation. Functionally, this switch resulted in a reduced production of reactive oxygen species (– 50%) in cardiomyocytes and an inotropic response (+ 18%) in transduced engineered heart tissues. Importantly, we could show that an adeno-associated virus 9-mediated overexpression of RGS3L in rats *in vivo*, increased the contractility of ventricular strips by maximally about twofold. Mechanistically, we demonstrate that this switch is mediated by a complex formation of RGS3L with the GTPase-activating protein p190RhoGAP, which balances the activity of RhoA and Rac1 by altering its substrate preference in cardiomyocytes. Enhancement of this complex formation could open new possibilities in the regulation of the contractility of the diseased heart.

**Keywords** Cardiac contractility · p190RhoGAP · RacGAP · Regulator of G protein signaling · RhoA

Susanne Lutz and Thomas Wieland share the senior authorship.

✉ Thomas Wieland  
thomas.wieland@medma.uni-heidelberg.de

- 1 Experimental Pharmacology Mannheim (EPM), European Center for Angioscience (ECAS), Medical Faculty Mannheim, Heidelberg University, Ludolf-Krehl-Str. 13-17, 68167 Mannheim, Germany
- 2 Department of Pharmacology, Center for Heart Failure Research, Institute of Clinical Medicine, University of Oslo and Oslo University Hospital, Oslo, Norway
- 3 Department of Cardiology, Heidelberg University, Heidelberg, Germany
- 4 Department of Experimental Pharmacology and Toxicology, University Medical Center Hamburg-Eppendorf, Hamburg, Germany
- 5 Institute of Pharmacology and Toxicology, University Medical Center Göttingen, Göttingen, Germany
- 6 Medical Department III, Christian-Albrechts-Universität Zu Kiel (CAU), Kiel, Germany
- 7 DZHK, German Center for Cardiovascular Research, Partner Sites Göttingen, Heidelberg/Mannheim and Hamburg/Kiel/Lübeck  
<https://dzhk.de>

## Introduction

G-protein-coupled receptors (GPCR) and their regulators are involved in numerous signaling processes in cardiovascular physiology including heart rate, conduction velocity, contractility, and vascular tone [82]. Perturbations in GPCR signaling contribute to pathological developments, such as heart failure, which is one of the leading causes of morbidity and mortality worldwide [67]. Despite evidence for the existence of all five muscarinic acetylcholine receptor subtypes in the heart, the M<sub>2</sub> muscarinic acetylcholine receptor (M<sub>2</sub>R) is the quantitatively dominant isoform in cardiac tissues [9, 22, 88].

M<sub>2</sub>Rs are known as inhibitory receptors of cardiac function by reducing heart rate and conduction velocity. In addition, they counteract the β-adrenoceptor-mediated increase in contractile force (accentuated antagonism) [25, 42]. Several studies have investigated the effect of vagal nerve stimulation in animal heart failure models or in human heart disease [29, 34, 44]. While reducing the heart rate is protective to the damaged heart and thus aimed for in heart failure therapy, a long lasting negative inotropic response due to M<sub>2</sub>R activation in the ventricles [55] would be detrimental.

Moreover, at least in the healthy rats, a chronic infusion of the muscarinic acetylcholine receptor agonist carbachol sensitizes the myocardium to cAMP-induced arrhythmia, most likely by reducing the amount of pertussis toxin (PTX)-sensitive  $G_i$  proteins in cardiomyocytes [18, 63]. Interestingly, however, activation of the  $M_2R$  caused a Rho-associated protein kinase (ROCK)-mediated inotropic response in an experimental model in the rat based on coronary artery ligation induced infarct and heart failure as well as in the neonatal rat heart [30, 40].

$M_2R$  signaling is under the control of various regulatory proteins. Regulators of G Protein Signaling (RGS) belong to a diverse family of GTPase-activating proteins (GAP), capable of accelerating GTP hydrolysis of the  $G\alpha$  subunit of heterotrimeric G proteins. Consequently, they are important negative regulators of canonical GPCR signaling pathways. RGS proteins have emerged as potential therapeutic targets due to their function in cardiovascular physiology and pathology [89, 94]. RGS3, which belongs to the R4 RGS protein subfamily, exists in several splice variants. RGS3L, a long isoform of RGS3 (519 amino acids), has in addition to the RGS domain an extended N-terminal segment, which enables interactions with other proteins, such as  $G\beta\gamma$ -dimers. Therefore, RGS3L acts not only as a GAP for the  $G\alpha$  proteins, but is also able to regulate the  $G\beta\gamma$ -mediated signaling by acting as a  $G\beta\gamma$  scavenger [73]. Several RGS3 isoforms, including RGS3L, are expressed in the human heart [56] and RGS3L mRNA and protein levels were upregulated in human heart failure [61]. Fibroblast growth factor 2 (FGF2), a known cardioprotective stimulus, increases RGS3L expression in rat cardiomyocytes [96]. Our group has reported previously, that RGS3L, besides its GAP activity towards  $G_i$  protein, is able to switch the  $M_2R$  signaling from Rac1 to RhoA activation in the model of  $M_2R$  expressing human embryonic kidney (HEK) cells as well as neonatal rat cardiomyocyte derived H10 cells [87]. However, the underlying molecular mechanism causing this switch is still unclear and the role of RGS3L in native cardiomyocytes has not been studied.

Like heterotrimeric G-proteins, monomeric GTPases of the Rho family, including Rac1 and RhoA, are active in the GTP-bound conformation and inactive in the GDP-bound state. Besides guanine nucleotide exchange factors (GEFs), GAPs are similarly important regulators of monomeric GTPases. GAPs largely accelerate the intrinsic GTPase activity of the small G proteins, and as a result terminate their signaling [86]. p190RhoGAP, a 190 kDa GTPase-activating protein expressed in the heart [72], is a regulator that balances Rac1 and RhoA activities in the cell [26, 71, 72, 90]. Although first described as a GAP specific for RhoA, it became evident that p190RhoGAP can also exhibit GAP activity towards Rac1 and even switch its substrate preference between RhoA and Rac1 [39, 41, 46].

We there performed an explorative study, which will provide evidence that the RGS3L expression level determines whether carbachol stimulation preferentially activates Rac1 or RhoA in cardiomyocytes by inducing an RGS3L/p190RhoGAP complex formation, which switches the GAP activity towards Rac1 and thus increases the amount of active RhoA. We will further demonstrate that this mechanism allows for the observed ROCK-mediated inotropic response upon carbachol stimulation in the rat ventricle.

## Materials and methods

### Antibodies, reagents, and inhibitors

We used the following primary antibodies: mouse-anti-Rac1 (BD Transd. Laboratories, 610650), mouse-anti-p190A (BD Transd. Laboratories, 610149), mouse-anti-RhoA (26C4, Santa Cruz, sc-418), mouse-anti-RGS3 (CC-Q7, Santa Cruz, sc-100762), rabbit-anti-Tiam1 (C-16, Santa Cruz, sc-872), rabbit-anti- $G\beta$  (T-20, Santa Cruz, sc-378), rabbit-anti-RGS3 (Abcam, ab2564), mouse-anti-c-myc (Klon 9E10, Oncogene), mouse-anti- $\beta$ -actin (Sigma-Aldrich, A2228), mouse-anti-RhoA-GTP (Biomol). The corresponding horseradish peroxidase-conjugated secondary antibodies were from Sigma-Aldrich (Saint Louis, MO, USA, A-9044, A-9169), the fluorescent labelled secondary antibodies (anti-mouse-Alexa Fluor® 568-antibody, anti-rabbit-Alexa Fluor® 633-antibody) were from Life Technologies. In this study, the following reagents and inhibitors were used: FGF-2 (Promega), carbamoylcholine chloride (carbachol), 5-bromo-2'-deoxyuridine (5-BrdU) (Sigma-Aldrich), PI3K-inhibitor LY294002 (2-(4-morpholinyl)-8-phenyl-1(4H)-benzopyran-4-one hydrochloride; Alexis), pertussis toxin (PTX; Calbiochem), H1152P ((S)-(+)-2-Methyl-1-[(4-methyl-5-isoquinolyl)sulfonyl]homopiperazine, 2HCl, Merck).

### Animal experiments and cell isolation from animals

All the experiments were performed according to the EU animal experiments guidelines and ethical approval by the local German ethics committee (G237/12, Regierungspräsidium Karlsruhe).

### Isolation and culture of neonatal rat cardiomyocytes (NRCM)

NRCM were isolated from hearts of 1–3-day-old male and female neonatal Wistar rats as described previously [92]. Briefly, hearts were minced and subjected to serial digestion in a mixture of collagenase (0.5 mg/ml collagenase type II, Cell systems) and pancreatin (0.6 mg/ml, Sigma-Aldrich) to release single cells. The obtained cell suspension was placed

on top of a Percoll gradient (GE Healthcare) to separate cardiomyocytes from other cell types. The cardiomyocyte fraction was seeded on collagen I-coated plates and cultured in DMEM supplemented with 10% (w/v) fetal calf serum, 2 mM L-glutamine, 100 units/ml penicillin and 100 µg/ml streptomycin in a humidified atmosphere of 5% CO<sub>2</sub> at 37 °C. 0.1 mM 5-BrdU was used to prevent overgrowth of other, non-cardiomyocyte cell types. The cells were used for experiments between 3 and 5 days after isolation. Serum-reduced conditions (DMEM supplemented with 0.5% FCS) were used for 48 h when indicated.

### Cell culture and transfection

HEK-293 cells were grown in Dulbecco's modified Eagle's medium (DMEM, Invitrogen) supplemented with 10% (w/v) fetal bovine serum, 2 mM L-glutamine, 100 units/ml penicillin and 100 µg/ml streptomycin in a humidified atmosphere of 5% CO<sub>2</sub> at 37 °C. Transient overnight transfection of the cells with p190RhoGAP, full length RGS3L-N460A, RGS3L or truncated RGS3L constructs were performed using Polyfect (Qiagen) transfection reagent according to the manufacturer's instructions. Cells were incubated under serum-reduced conditions and investigated 24–48 h after transfection. The measurement the RacGAP and RhoGAP activity of p190RhoGAP was performed using a pulldown assay described below.

The HEK-293 cells were from Agilent and routinely monitored for possible mycoplasma contamination.

### Generation of recombinant adenoviruses

The coding sequences of RGS3L and RGS3L-N460A were subcloned into the adenoviral shuttle vector pAdTrack-CMV (a gift from Dr. B. Vogelstein, Baltimore, MD). The cDNA oligonucleotide 5'-ATCCCGGAAGGAATCCTTTTCAGGTTCAAGAGAACTGAAAAGGAT-TCCTTCCTTTTGGAAA-3' encoding the RGS3L-shRNA sequence was subcloned into the BglIII/HindIII sites of the pShuttle H1 vector (Stratagene). For knockdown of Tiam1 the cDNA oligonucleotide 5'GATCCCGCGAGCTTTAAGAAGAACTTCAAGAGAGTTTCTTCTTAA-AGCTCGCTTTTGGAAA-3' encoding Tiam1-shRNA was used. The complete H1 promoter driven expression cassette was subcloned into pAdTrack [12]. After recombination of the created shuttle vectors with pAdEasy-1, the Pac I linearized recombinant adenoviral genome was transfected and amplified in HEK-293 cells.

### Generation of AAV-9 viruses

The cDNA sequences of the variant/mutant RGS3L-N460A was cloned into a single-stranded AAV genome plasmid

(pSSV9-CMV-MLC1500-luc) via XbaI restriction replacing the luciferase (luc) gene. The correct fragment size and orientation was controlled by agarose gel-electrophoresis and sequencing resulting in pSSV9-CMV-MLC1500-RGS3L-N460A. AAV9 vectors were generated by double-transfection of helper plasmid pDP9rs [79] and either pSSV9-CMV-MLC1500-RGS3L-N460A or -luciferase (as control). Vectors were then purified using iodixanol step gradient ultracentrifugation followed by genomic titer determination using quantitative real-time PCR as described previously [31].

### 2D gel electrophoresis

Cell lysates (about 50 µg protein) were mixed with 70 µl rehydration buffer and applied to 7 cm IPG gel strips (GE Healthcare) containing a linear 3–10 pH gradient. Isoelectric focusing was carried out using an Ettan IPGphor unit (GE Healthcare). The subsequent SDS-PAGE was performed on 8% polyacrylamide gels.

### Immunoblot analysis

For immunoblot analysis the protein samples were separated by SDS-PAGE using 8–15% denaturing acrylamide gels and transferred onto nitrocellulose membranes. Membranes were blocked with Roti-Block (Carl Roth) for 1 h at room temperature, and incubated with specific primary antibodies (see above) overnight at 4 °C and according to the manufacturer's recommendations. After incubation with appropriate secondary antibodies for 1 h, proteins were visualized by enhanced chemoluminescence using an imaging system (Alpha Innotech). Image J Software was used for the analysis of the blots.

### Rac and RhoGTPase activation assay

The cellular Rac1-GTP and RhoA-GTP levels were measured with a pull-down assay using GST fusion proteins containing the Rho-binding domain of rho-kinase (GST-RBD) or Rac-binding domain of p21-activated kinase (PAK1) (GST-PBD). GST-RBD and GST-PBD were expressed and purified from *E. coli*. NRCM were stimulated with FGF2 or transduced with adenoviruses and pretreated with the different inhibitors described above. After activation of the NRCM with carbachol (1 mM, 5 min), cells were lysed in ice-cold GST-Fish buffer [11, 87] and pelleted by centrifugation (12,000 rpm, 3 min at 4 °C). The GTP-bound RhoGTPases contained in the supernatant was incubated for 1 h at 4 °C with either GST-PBD bound to magnetic glutathione-sepharose beads or GST-RBD bound to non-magnetic glutathione-sepharose beads. The beads were separated using a magnetic plate and centrifugation. After

twice washing of the beads, bound proteins were eluted with sample buffer and separated by SDS–PAGE. The amounts of activated GTPases and total GTPases from lysates as loading control were then determined by immunoblot analysis as described above.

### Measurement of reactive oxygen species (ROS) in NRCM

NRCM were cultured on 96-well plates (Sarstedt). The cells were transduced with shEGFP, shTiam or RGS3L–N460A encoding adenoviruses, and treated with FGF2 or PTX as described above. Thereafter, the cells were stimulated with 1 mM carbachol or solvent for 5 min at 37 °C. Myocytes were then loaded for 30 min with 5  $\mu$ M 5(6)-carboxy-2',7'-dichlorofluorescein (DCF-DA, Sigma-Aldrich) at 37 °C. After washing the cells with HEPES buffered salt solution (HBSS; 25 mM HEPES pH 7.4, 120 mM NaCl, 5.4 mM KCl, 1.8 mM CaCl<sub>2</sub>, 25 mM NaHCO<sub>3</sub>, 15 mM Glucose), DCF fluorescence was measured using the Envision 2102 Multilabel Reader with a set of FITC filters (excitation 485  $\pm$  10 nM and emission at 535  $\pm$  20 nM, PerkinElmer).

### MLC-2 phosphorylation

NRCM were transduced with EGFP (control) or RGS3L–N460A encoding adenovirus for 24 h, treated with 100 nM H1152P for 1 h as indicated and stimulated with 1 mM carbachol or solvent for 90 s at 37 °C. Thereafter, the cells were lysed in a buffer containing phosphatase inhibitor PhosStop (Roche Applied Science). The lysates were cleared by centrifugation and subjected to SDS–PAGE and immunodetection. Finally, densitometric band intensities of pMLC-2 were quantitated using total MLC-2a as control.

### Immunoprecipitation

NRCM were transduced with RGS3L–N460A adenovirus for 24 h and stimulated with 1 mM carbachol or solvent for 5 min at 37 °C. Co-immunoprecipitation was performed as described previously [5]. Briefly cells were lysed with immunoprecipitation buffer (50 mM Tris–HCl, pH 7.4, 2 mM EDTA, 150 mM NaCl, 0.1% SDS, 1% Nonidet P-40, 10 mM NaF) containing 1 mM sodium orthovanadate, 1 mM Pefablock, 10  $\mu$ g/ml aprotinin, 10  $\mu$ g/ml leupeptin). After centrifugation the cleared lysates were incubated with the indicated antibodies (2  $\mu$ g) under agitation for 1 h at 4 °C. After addition of 40  $\mu$ l 1:1 (v/v) protein-A–sepharose-beads (Amersham Biosciences), the mixture was gently shaken for an additional 3–4 h at 4 °C. Beads were washed three times with immunoprecipitation buffer and eluted in SDS-containing buffer for 5 min at 95 °C. After SDS–PAGE and transfer to nitrocellulose membranes, immunoprecipitated proteins

were detected by Western blot analysis using the indicated antibodies according to standard protocols. Final detection was done with an ECL system (Amersham), band intensity was quantified with ImageJ-software.

### Proximity ligation assay (PLA)

Proximity ligation assay was performed by following the manufacturer's protocol (Olink Bioscience, Uppsala, Sweden). Briefly, NRCM seeded on collagen-coated coverslips in 12-well dishes were stimulated with or without carbachol for 5 min, washed 3 times with PBS, fixed in 4% formaldehyde in PBS for 10 min, permeabilized in 0.02% Triton-X-100 for 10 min, and blocked with Blocking Solution (Olink) for 30 min in 37 °C. After incubation with the indicated primary antibodies (mouse–anti-p190RhoGAP, rabbit–anti-RGS3) over night at 4 °C, wells were washed with Wash Buffer (Olink), incubated with PLA Probe anti-mouse plus and PLA Probe anti-rabbit minus for 1 h at 37 °C. After washing, a ligation and amplification step followed using the manufacturer's protocol and reagents. Cells were mounted with Duolink In Situ Mounting Medium with DAPI, dried in room temperature and visualized by confocal microscopy (Leica, Germany). The LAS-X software was used for image processing. Quantification of fluorescent signals was performed using Image J software.

### Measurement of the GAP activity of p190RhoGAP towards Rac1 and RhoA

Measurement of the functional RhoGAP activity of p190RhoGAP was performed by a pulldown assay as described previously [5, 58]. This assay is based on the principle that the functional activation of p190RhoGAP is indicated by an increased ability to associate with its substrate, the active, GTP-bound form of monomeric GTPases. The ability of p190RhoGAP to act as a RhoAGAP was detected using constitutively active RhoAQ63L-GST coated beads. The more p190RhoGAP protein binds to the beads, the higher is its RhoAGAP activity (corresponding to a decreased level of RhoA-GTP in the cell [58]). Using RacQ61L-GST-coated beads instead the Rac1GAP-activity of p190RhoGAP can be measured. Briefly, cells (NRCM or HEK-293 cells) were washed carefully with PBS and lysed in a buffer containing 50 mM Tris–HCl, pH 7.4, 10 mM MgCl<sub>2</sub>, 150 mM NaCl, 1 mM DTT, 1% Triton X-100, 10 g/ml each of aprotinin and leupeptin, 1 mM Pefablock and 1  $\times$  Phosstop (Roche). After centrifugation for 3 min at 12,000 $\times$ g, the supernatants were incubated for 60 min at 4 °C with glutathione–sepharose magnetic beads coated with RhoQ63L or RacQ61L conjugated with GST and purified previously from Rosetta *E. coli* bacteria. The beads were separated using a magnetic plate. After three times washing

of the beads, bound proteins were eluted with sample buffer and separated by SDS–PAGE. p190RhoGAP was detected by immunoblotting.

### Immunocytochemistry

Subconfluent NRMC were cultured on 12 well plates (Sarstedt), washed three times with PBS and fixed with 3% paraformaldehyde/PBS for 15 min at room temperature. After the cells were treated with 0.05% Triton-X-100 for 3 min at room temperature and 0.5% bovine serum albumine (BSA) for 45 min at 4 °C, they were incubated with the appropriate antibodies for 16 h at 4 °C. After washing with PBS, the cells were incubated with the indicated secondary antibodies for 1 h at room temperature. Images of the cells mounted at room temperature in PBS were acquired using fluorescence microscopy (Olympus IX 81).

### Isolation and culture of adult mouse ventricular cardiomyocytes (AMVCM)

Ventricular myocytes of adult mice were isolated by retrograde Langendorff perfusion using an enzyme composition of collagenase type I and II, dispase (Liberase DH, Roche) and trypsin. The protocol for the isolation of adult ventricular cardiomyocytes was modified from Borner et al. [8]. The mice (age of 10–20 weeks) were anesthetized with 2% isoflurane in oxygen and sacrificed by cervical dislocation. After fixation on a Styrofoam plate and disinfection with 70% ethanol, the thorax was opened. The heart was isolated by cutting distal from the heart, close to the aortic arch and was directly transferred into ice-cold perfusion buffer. The aorta was cannulated with a buffer-filled modified 20G cannula. The heart was connected to the pre-heated (37 °C) perfusion system with a flow of 3.5 ml per min and washed for 30 s. After perfusion with 29.6 mL of digestion buffer, the ventricles were separated from the atria, and cut into 1–2 mm<sup>3</sup> pieces in 2.5 ml digestion buffer. Digestion was stopped with 2.5 ml stopping buffer 1 and the tissue was titrated with a wide opening syringe. Undigested tissue was removed by sedimentation, and the isolated cells were resuspended in 4.75 ml stopping buffer 2. Recalcification was performed by in five steps until a final concentration of 960 μM CaCl<sub>2</sub> was reached. The cells were allowed to sediment by gravity and were then resuspended in fresh pre-warmed adult mouse cardiomyocyte medium. The cardiomyocytes were plated in droplets on laminin-coated glass cover slips (Ø 18 mm) in a 12-well plate or seeded in uncoated 6-well plates and were incubated for 30 min at 37 °C and 5% CO<sub>2</sub>. Unattached cells were removed, and fresh medium was added. The attached cardiomyocytes were cultured for 24 to 48 h at 37 °C and 5% CO<sub>2</sub>. (Buffers and media: Stock perfusion buffer 10 × pH 7.4, 1.13 M NaCl, 47 mM KCl, 6 mM

KH<sub>2</sub>PO<sub>4</sub>, 6 mM Na<sub>2</sub>HPO<sub>4</sub> × 2 H<sub>2</sub>O, 12 mM MgSO<sub>4</sub> × 7 H<sub>2</sub>O, 100 mM KHCO<sub>3</sub>, 100 mM HEPES; Perfusion buffer 1 x: 10% (v/v) Stock perfusion buffer 10 x, 23 mM NaHCO<sub>3</sub>, 30 mM taurine, 5.5 mM glucose, 9.9 mM BDM; liberase solution: 0.4% (w/v) liberase DH in ddH<sub>2</sub>O; Digestion buffer: 29.6 ml Perfusion buffer 1 x, 3.75 μl CaCl<sub>2</sub> 100 mM, 450 μl liberase solution, 200 μl Trypsin 2.5%; Stopping buffer stock solution: 1% (w/v) BSA 10 mL, Perfusion buffer 1 x; Stopping buffer 1: 2.25 ml Stopping buffer, 1.25 μl CaCl<sub>2</sub> 100 mM; Stopping buffer 2: 4.75 ml Stopping buffer, 1.9 μl CaCl 100 mM; Culture medium AVMCM MEM, 0.25% (v/v) (–)-blebbistatin (0.5 mM), 1% (w/v) BSA, 1% (v/v) P/S, 1% (v/v) L-glutamine (200 mM), 1% (v/v) ITS-X, laminin solution: 0.01% (w/v) in AMCM-medium).

### Measurement of the RhoA activity in adult mouse cardiomyocytes

Measurement of the RhoA-activity in AVMCM was performed by immunofluorescence staining using anti-RhoA–GTP-antibody, microscope image acquisition, and quantification of fluorescence. Cells isolated from mouse hearts were seeded on collagen-coated coverslips in 12-well dishes in Modified Eagle Medium (MEM) supplemented with 1% BSA, 100 units/ml penicillin and 100 μg/ml streptomycin, 1% L-glutamine, 1% (–) blebbistatin, 1% ITS (insulin–transferrin–selenium) in a humidified atmosphere of 5% CO<sub>2</sub> at 37 °C. Cells were transduced with Myc-tagged RGS3L–N460A–adenovirus or control EGFP–adenovirus for 48 h. After stimulation with or without 1 mM carbachol for 5 min, cells were fixed in 4% formaldehyde in PBS for 10 min, permeabilized and blocked for 10 min in a blocking buffer containing 10% FCS, 0.2% Triton-X 100 in Ca<sup>2+</sup>- and Mg<sup>2+</sup>-free PBS. Incubation with primary antibodies (mouse–anti-RhoA–GTP-antibody 1:500, rabbit–anti-c-myc-antibody 1:100) was performed in blocking buffer over night at 4 °C. After washing with PBS, cells were incubated with the corresponding fluorochrome-labeled secondary antibodies (anti-mouse-Alexa Fluor 568-antibody 1:1000, anti-rabbit-Alexa Fluor 633-antibody 1:1000) over night at 4 °C, and washed thereafter with PBS. DAPI (1:1000 in PBS for 1 h) was used to detect nuclei. After washing with PBS and mounting, coverslips were dried at room temperature. Cells were visualized by confocal microscopy (Leica, Germany), software LAS-X was used for image processing. Analysis of the fluorescence intensity of the Alexa Fluor 568 conjugate was performed using Image J (Version 1.47v).

### Preparation of EHT and measurement of the contractility of EHT

Neonatal rat engineered heart tissues (EHT) were generated and analyzed as previously reported [24]. In brief, agarose

casting molds were prepared in 24 well plates (NUNC) with liquid agarose (2% (w/v), PBS) and polytetrafluorethylen (PTFE) spacer. After agarose solidification PTFE spacer were removed and polydimethylsiloxan (PDMS) were placed on the 24 well plate so that pairs of flexible PDMS posts reach into each agarose casting mold. Dissociated neonatal rat heart cells were re-suspended in a fibrinogen solution (5 mg/ml). 97  $\mu$ l were mixed with 3  $\mu$ l thrombin aliquot (100 U/ml) and pipetted into a casting mold. This pipetting step was repeated for each EHT. Fibrin polymerization took place in an incubator (2 h) and PDMS racks with fibrin gels attached to the PDMS posts were transferred to new 24 well plates. EHT were cultivated in maintenance media (DMEM, Horse serum 10% (v/v), insulin 10  $\mu$ g/ml, aprotinin 33  $\mu$ g/ml) with media replacement on Mondays, Wednesdays and Fridays. After development (days 25–30) EHT were transferred to modified Tyrode's solution containing 0.1 mM free  $\text{Ca}^{2+}$  (120 mM NaCl, 22.6 mM  $\text{NaHCO}_3$ , 5.4 mM KCl, 5 mM glucose, 1 mM  $\text{MgCl}_2$ , 0.4 mM  $\text{NaH}_2\text{PO}_4$ , 0.1 mM  $\text{CaCl}_2$ , 0.05 mM  $\text{Na}_2\text{EDTA}$ , 25 mM HEPES) and force analysis was performed by video-optical recording of EHT shortening as recently described [24].

### Injection of the AAV9 virus and preparation of rat ventricular muscle strips

The care and experimental use of all animals in this study were in accordance with institutional guidelines and approved by the local ethics committee (Regierungspraesidium Karlsruhe).

We injected 6-week-old male Wistar rats with AAV9-CMV-MLC1500-RGS3L-N460A-virus or with an AAV9-CMV-MLC1500-luc control virus ( $10^{12}$  vg/rat) intravenously. After 2 months, the rats were anaesthetized (2–3% isoflurane flow) and subsequently euthanized by cervical dislocation. The hearts were harvested and mounted on a Langendorff rig perfused with a relaxing solution containing 118.3 mM NaCl, 3 mM KCl, 0.2 mM  $\text{CaCl}_2$ , 4 mM  $\text{MgSO}_4$ , 2.4 mM  $\text{KH}_2\text{PO}_4$ , 24.9 mM  $\text{NaHCO}_3$ , 10 mM glucose and 2.2 mM mannitol [77]. The left ventricle was exposed and posterior left ventricular papillary muscles and strips of left ventricles (approx. 1 mm diameter) were excised and mounted in organ baths (Radnoti organ bath System, ADInstruments) containing the relaxing solution (32 °C) as described above and oxygenated (95%  $\text{O}_2$ , 5%  $\text{CO}_2$ ).

### Measurement of the contractility of the isolated rat papillary muscle strips

After mounting, the strips were stretched to ~3 mN diastolic tension, allowed to relax ~5 min and then the relaxing solution was replaced with a solution of identical composition

with the exception of 1.8 mM  $\text{CaCl}_2$  and 1.2 mM  $\text{MgSO}_4$  concentrations. The muscle strips were field stimulated at a frequency of 1 Hz with impulses of 5 ms duration and current about 10–20 mA. The isometrically contracting muscles were stretched to the maximum of their length–tension curve. Contraction–relaxation cycles were recorded and analyzed as previously described [75, 76]. Basal contractility was expressed as maximal developed force ( $F_{\text{max}}$ , mN). The descriptive parameters at the end of the equilibration period were used as basal (control) values. Inotropic responses were expressed as changes in the maximal development of force ( $(dF/dt)_{\text{max}}$ ). The measurements were based on averaging 10–20 contraction–relaxation cycles. Antagonists of  $\alpha$ 1-adrenoceptors (prazosin 1  $\mu$ M) and  $\beta$ -adrenoceptors (timolol 1  $\mu$ M) were added 90 min before the muscarinic agonist carbachol which was added to the organ bath as a bolus (100  $\mu$ M). The contractility measurements were conducted at increasing extracellular  $\text{Ca}^{2+}$ -concentrations (ranging from 1.8 to 3.0 mM).

### Statistical analysis

Exploratory data analysis was performed using the GraphPad Prism software (GraphPad Software, Version 6, La Jolla). Data were expressed as mean  $\pm$  SD. If not otherwise, indicated Student's *t* test or one-way-ANOVA with Tukey's multiple comparison test were performed. A *p* value < 0.05 was considered statistically significant.

## Results

### The RGS3L expression level determines RhoGTPase activation in NRCM upon stimulation with carbachol

FGF2 increases RGS3 expression in neonatal rat cardiomyocytes (NRCM) [96] and the level of RGS3L determines the  $\text{M}_2\text{R}$  coupling to Rac1 or RhoA in H10 cells [87]. Therefore, we analyzed RGS3 expression with and without FGF2 treatment and its effect on RhoGTPase activation in NRCM. As established before [87], we used 2D gel electrophoresis with subsequent immunoblotting to identify specific isoforms of RGS3. RGS3L was detected at the predicted isoelectric point (pI) and molecular mass of 4.79 and 61 kDa, respectively (Fig. 1A). In accordance with the published data [91], a marked increase in the amount of RGS3L protein was detected in NRCM treated with FGF2 for 24 h. Next, we examined the activation of Rac1 and RhoA in FGF2-treated NRCM in response to carbachol. Under control condition carbachol caused a prominent Rac1 and a weak RhoA activation, whereas in FGF2-treated cells the opposite was found (Fig. 1B, C). Both the carbachol-induced Rac1 and

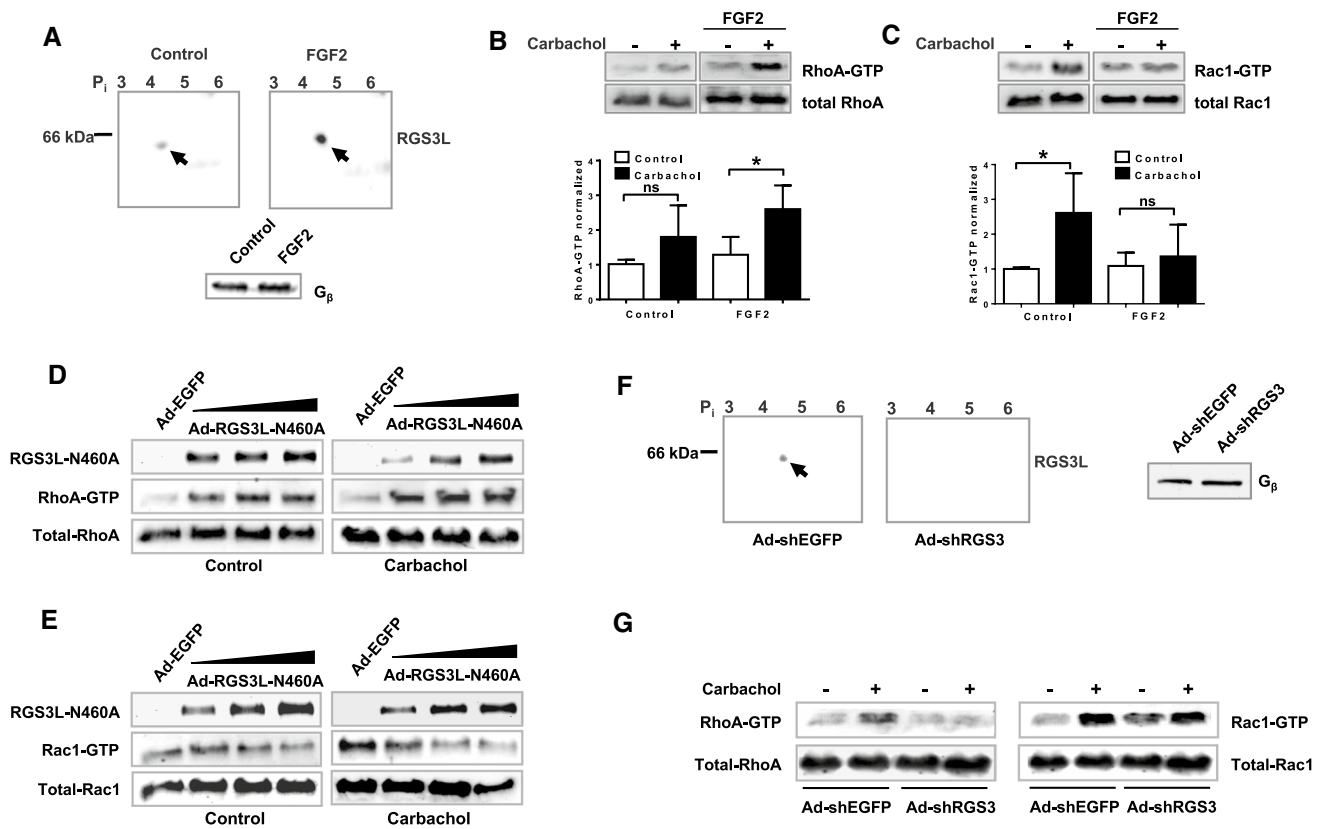


**Fig. 1** Effect of the expression level of RGS3L on the carbachol-induced RhoGTPase activation in NRCM. **A** Identification of the specific RGS3 isoform expressed in NRCMs treated under serum-free conditions with or without 50 ng/ml FGF2 for 24 h, as indicated. RGS3 in the cell lysates was analyzed by 2D gel electrophoresis and immunoblot.  $G_{\beta}$  was used as a loading control (**B**, **C**). Measurement of the carbachol-induced RhoA (**B**) and Rac1 activation (**C**) in NRCMs without or with FGF2 treatment stimulated without and with 1 mM carbachol for 5 min. Levels of Rac1-GTP and RhoA-GTP were measured by Rac1 and RhoA activation assays. Quantification of Rac1 (Rac-GTP/total Rac1) and RhoA activity (RhoA-GTP/total RhoA) as well as a representative experiment are shown. The mean of

Rac1-GTP or RhoA-GTP levels detected in unstimulated cells was set to 1.0. Values are mean  $\pm$  SD ( $n=8/5$  RhoA/Rac1),  $*p < 0.05$ . **D**, **E** NRCMs were transduced with Ad-EGFP (Control, MOI 40) and increasing amounts (MOI 10, 20, 30) of Ad-RGS3L-N460A for 48 h. Levels of RhoA-GTP (**D**) and Rac1-GTP (**E**) were determined after 5 min stimulation without or with carbachol. Recombinant RGS3L expression was monitored by immunoblot analysis using the anti-c-myc antibody. **F**, **G** NRCMs were transduced with Ad-shEGFP [12] and Ad-shRGS3L for 72 h. RGS3L expression was monitored by 2D gel electrophoresis and immunoblot.  $G_{\beta}$  was used as a loading control. **F** Cells were incubated for 5 min with or without carbachol. Levels of RhoA-GTP and Rac1-GTP were determined

RhoA activations were reduced by treatment with PTX or the phosphoinositide-3-kinase (PI3K) inhibitor LY294002 independent of FGF2 (Supplemental Fig S1A). These data are in accordance with the  $G_i$ - and PI3K-dependent RhoA and Rac1 activation observed in carbachol-treated NRCM-derived H10 cells and thus indicate the existence of a similar signaling pathway in primary NRCM [87].

To verify the dependence between the expression level of RGS3L and the coordinated activation of either RhoA or Rac1 in NRCM, we altered RGS3L expression using different experimental approaches. First, we transduced NRCM with an adenovirus encoding the GAP-deficient RGS3L mutant RGS3L-N460A, which mediated in  $M_2R$  expressing cells a prolonged carbachol-induced RhoA activation compared to wild-type RGS3L [87]. Increasing expression of RGS3L-N460A in NRCM induced a pronounced

RhoA activation in the absence and presence of carbachol (Fig. 1D). In addition, the increasing expression of RGS3L-N460A preferentially suppressed the carbachol-stimulated Rac1 activation (Fig. 1E). Second, loss of function experiments were performed by transducing NRCM with an adenovirus encoding a shRNA directed specifically against RGS3L (Ad-shRGS3L) [15]. As shown in Fig. 1F, the expression of RGS3L was nearly abolished in the Ad-shRGS3L-transduced NRCM compared to cells transduced with a control adenovirus encoding for a shRNA against EGFP.  $G_{\beta}$ , which served as a loading control, remained unaffected. Most importantly, RGS3L depletion reduced the carbachol-induced RhoA activation to control level (Fig. 1G). This effect was dependent on the virus load used for NRCM transduction (Supplemental Fig S1B). In contrast, the carbachol-induced Rac1 activity remained unchanged. In

summary, these data demonstrate that the expression level of RGS3L dynamically regulates RhoA activation in NRCM and determines whether Rac1 or RhoA activation prevails after carbachol application.

### **RGS3L increases carbachol-evoked MLC-2 phosphorylation in a ROCK-dependent manner**

In the neonatal rat heart as well as in an experimental heart failure model, the M<sub>2</sub>R-induced inotropic response was sensitive to ROCK inhibition and accompanied by increased MLC-2 phosphorylation [30, 40]. In NRCM, both the ventricular isoform MLC-2<sub>v</sub> and the atrial isoform MLC-2<sub>a</sub> are present and both localize along the myofilaments (Fig. 2A). To study the influence of RGS3L–N460A on the carbachol-induced MLC-2 phosphorylation, we used a polyclonal antibody against MLC-2a-P, which recognizes mono- and diphosphorylated (Ser22 and/or Ser23) MLC-2a. Treatment with carbachol in control-transduced NRCM slightly increased MLC-2 phosphorylation, which was, however, enhanced by the expression of RGS3L–N460A (Fig. 2B). The quantification of the carbachol-induced MLC-2 phosphorylation revealed a 33% increase in the presence of RGS3L–N460A compared to the non-stimulated cells (Fig. 2C). Treatment of the cells with the selective ROCK inhibitor H1152P completely blocked the carbachol-induced MLC-2 phosphorylation in the presence of RGS3L–N460A (Fig. 2B, C).

To study whether the increase in ROCK-mediated MLC phosphorylation is associated with an increase in contractility, rat engineered heart tissues (EHT) were prepared from neonatal rat heart cells. As shown in Fig. 2D, the EHT express detectable levels of RGS3L. In contractility measurements a moderate but statistically significant increase in contractile force was observed after carbachol stimulation (Fig. 2E). This inotropic response was blunted by adding the ROCK inhibitor H1152P (Fig. 2E), which is in accordance with the described carbachol-induced inotropy of the neonatal rat heart [40].

### **RGS3L increases the carbachol-induced RhoA activation at the sarcolemma of adult ventricular cardiomyocytes and the contractility in isolated ventricular muscle strips**

NRCMs are a widely used model to study cardiomyocyte signaling, nevertheless, they largely differ from fully differentiated adult cardiomyocytes with regard to myofilament and subcellular organization. Therefore, we studied whether RGS3L–N460A overexpression could also evoke RhoA activation in isolated adult mouse ventricular cardiomyocytes (AMVCM) in which RhoA activation was visualized by confocal microscopy using a specific anti-RhoA–GTP

antibody. In addition, the expression of RGS3L–N460A was monitored by immunofluorescence (Fig. 3A, B). Interestingly, we observed that RhoA–GTP and RGS3L–N460A co-localized at the sarcolemma of AMVCM. Moreover, carbachol treatment did not alter the RhoA–GTP level in control transduced AMVCM, but significantly increased it in RGS3L–N460A expressing AMVCM (Fig. 3C, D). These data demonstrate that higher RGS3L expression levels allow for a M<sub>2</sub>R-induced RhoA activation also in adult cardiomyocytes.

We, therefore, aimed to verify that high expression levels of RGS3L in cardiomyocytes allow for a carbachol-induced inotropic response in the healthy ventricular tissue. We injected 6-week-old male Wistar rats either with AAV9–CMV–MLC1500–RGS3L–N460A virus (AAV–RGS3L–N460A) or AAV9–ssCMV–MLC1500–luc control virus (AAV–luc). The animals were housed for a further 2 months prior to experimentation. They did not show any signs of distress and none died. After sacrifice, the hearts were explanted and cardiac contractility was measured *ex vivo* in ventricular muscle strips (Fig. 4). In line with the data reported before from failing rat hearts [30], carbachol initially decreased the contractility of control as well as RGS3L–N460A expressing muscle strips in a transient manner (Fig. 4C, D). In the RGS3L–N460A-expressing ventricular muscle strips, the return to baseline was accelerated, followed by an inotropic response significantly exceeding the baseline (Fig. 4D). This inotropy was more prominent at higher Ca<sup>2+</sup> concentrations and later timepoints (Fig. 4D–F). Plotting of the expression level of RGS3L–N460A vs. the measured force of contraction of the individual muscle strip revealed a statistically significant positive correlation between both parameters (Fig. 4G). These results suggest that the expression of RGS3L is indeed linked to the contractile response.

### **The RGS3L mediated switch from carbachol-induced Rac1 to RhoA activation requires a complex formation of RGS3L with p190RhoGAP**

RGS3L displays no GAP activity towards monomeric GTPases and thus likely influences the activity of RhoGTPases by interacting with either GEFs or GAPs. However, it was shown that its interference with G<sub>i</sub>-mediated Rac1 activation depends on its capacity to bind Gβγ dimers [87]. Previous studies reported that in NRCM the G<sub>i</sub>βγ/PI3K-induced activation of Rac1 via G<sub>i</sub>-protein-coupled receptors is mediated by the guanine nucleotide exchange factor Tiam1 [21, 85]. To investigate the role of Tiam1 in the carbachol-induced Rac1 as well as RhoA activation, we transduced NRCM with an adenovirus encoding a Tiam1-specific shRNA and studied the activation of RhoA and Rac1. As shown in Fig. 5, the expression of Tiam1 was



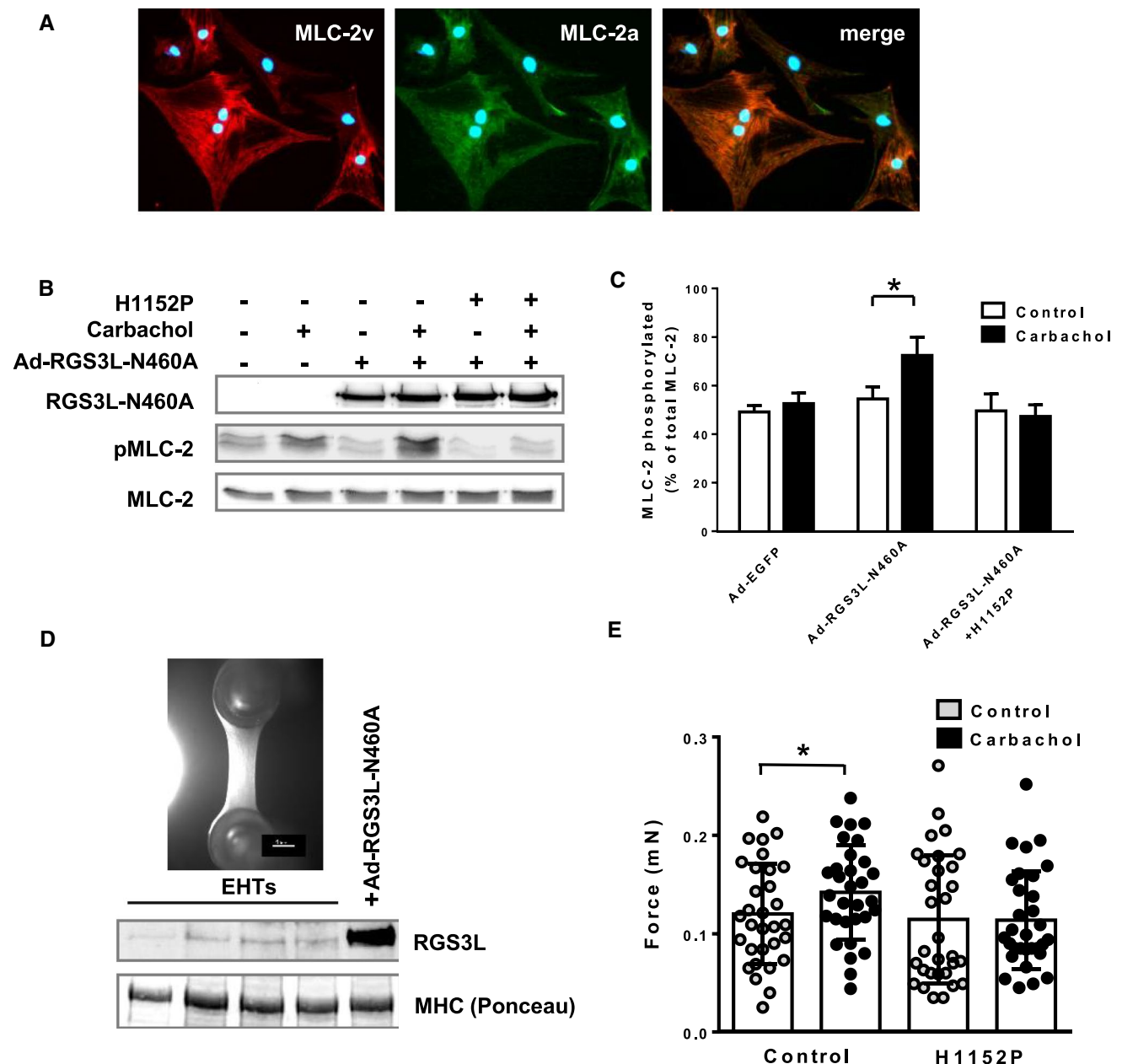


**Fig. 2** Effect of RGS3L-N460A expression on the carbachol-induced MLC-2 phosphorylation in NRCM and measurement of contractility in rat engineered heart tissue (EHT). **A** Detection of the ventricular isoform MLC-2v and the atrial isoform MLC-2a in NRCMs by immunocytochemistry. **B** NRCMs were transduced with Ad-RGS3L-N460A or Ad-EGFP and stimulated with or without carbachol for 5 min. The phosphorylation status of MLC-2 was analyzed by immunoblot using a polyclonal antibody against MLC-2a-P, which recognizes both, mono- and diphosphorylated (Ser22 and/or Ser23) MLC-2a. MLC-2a was used as a loading control. For ROCK-inhibition, cells were pretreated with 100 nM H1152P for 1 h. **C** Quantification

of the MLC-2 phosphorylation in NRCM relative to the total MLC-2 amount. Values are mean + SD ( $n=4-6$ ),  $*p < 0.05$ . **D** Expression of RGS3L in NRCM-derived EHT. Adenoviral overexpressed RGS3L-N460A in NRCM was used as a positive control. **E** EHT were stimulated with 50  $\mu$ M carbachol with and without treatment with 100 nM H1152P which was added 40 min before stimulation with carbachol. The analysis of the contraction force was performed by video-optical recording of EHT shortening. Statistical analysis was performed by repeated measures ANOVA with Sidak's multiple comparisons test. Values are mean + SD ( $n=31$ ),  $*p < 0.05$

largely reduced compared to cells transduced with a control shRNA encoding virus. The downregulation of Tiam1 abolished the carbachol-induced Rac1 activation (Fig. 5B)

as well as the carbachol-induced ROS production (Fig. 5C), which likely originates from the Rac1-dependent activation of NADPH oxidase in NRCM [1]. Consistent with this

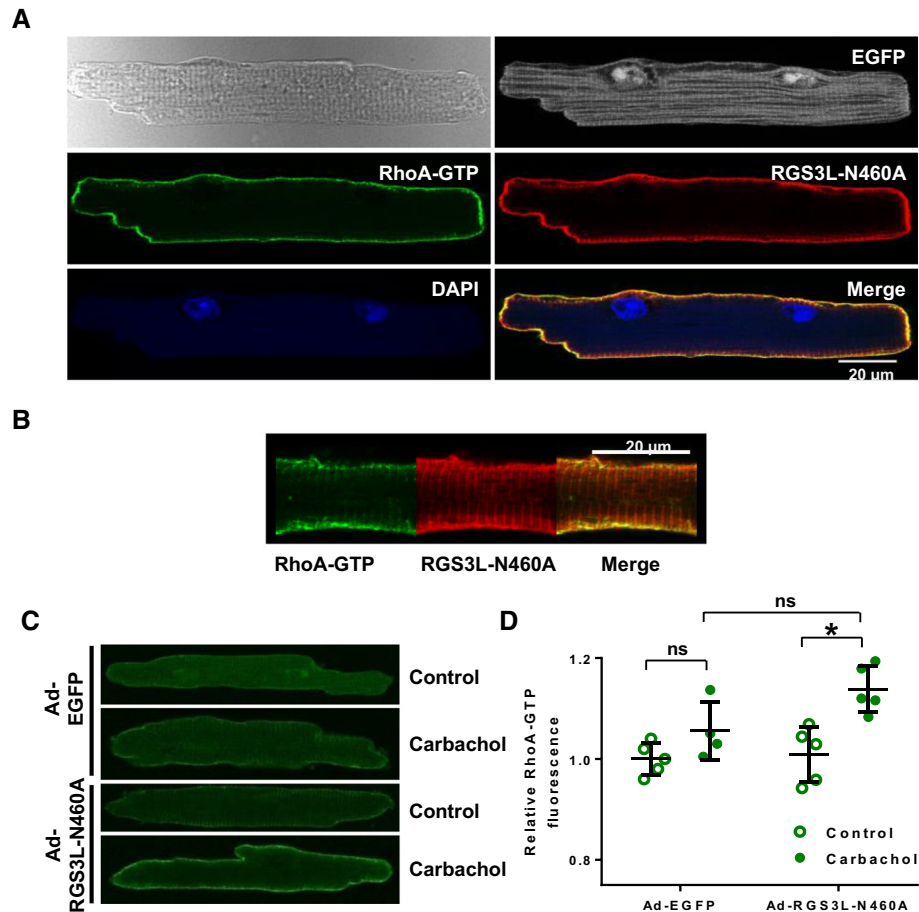


**Fig. 3** Effect of RGS3L–N460A expression on the  $M_2R$ -mediated RhoA activation in AMVCM. Cells were transduced with Ad-RGS3L–N460A or Ad-EGFP for 48 h. Cells were stimulated with or without carbachol for 5 min. RhoA–GTP was detected with mouse–anti-RhoA–GTP–antibody and secondary anti-mouse-Alexa Fluor<sup>®</sup> 568–antibody, RGS3L–N460A was detected using rabbit–anti-c-myc antibody and a secondary anti-rabbit-Alexa Fluor<sup>®</sup> 633–antibody. DAPI was used to detect nuclei. Sarcomeric proteins are visualized by a non-specific incorporation of EGFP. Cells were visualized by

confocal microscopy (Leica, Germany) and fluorescence at the sarcolemma was analyzed using ImageJ–software. **A**, **B** Localization of RhoA–GTP and RGS3L–N460A in AMVCM transduced with RGS3L–N460A adenovirus and stimulated with carbachol. Visualization of RhoA–GTP in representative cells (**C**) and analysis of the fluorescence intensity of the Alexa Fluor<sup>®</sup> 568 conjugate (which corresponds to the RhoA–GTP–amount) at the sarcolemma in 5 transductions obtained from 3 independent AMVCM preparations (**D**). Values are mean + SD, \* $p < 0.05$

interpretation, the carbachol-induced production of ROS was sensitive to PTX treatment, RGS3L–N460 overexpression, and FGF2, all suppressing the carbachol-induced Rac1 activation (Fig. 5D). In line with these data, the phenylephrine (PE)-induced protein synthesis, which requires a  $G_i\beta\gamma$ - and PI3K-dependent, Tiam1-mediated Rac1 activation [85], was suppressed by the overexpression of RGS3L–N460A (Fig. 5E). These data suggest that RGS3L could additionally protect the heart not only by reducing the Rac1 activity induced by carbachol, but also by interfering with other Rac1-dependent pathways involved in the development of cardiac hypertrophy. This interpretation is further supported by data showing that the hypertrophy induced by the inflammatory stimulus PGE2 through a Tiam1/Rac1-dependent activation of the transcription factor MEF2 could also be

suppressed by RGS3L [83]. Interestingly, the depletion of Tiam1 also abolished the carbachol-induced RhoA activation in the presence of RGS3L–N460A (Fig. 5B), indicating that Tiam1 is also essential in this pathway. Nevertheless, Tiam1 is a bona fide RacGEF. An exchange activity against RhoA has never been reported in a cellular context but it is a well-known protein–protein interaction partner integrating a variety of signaling proteins [7, 50]. As GAPs are as important for Rac1 and RhoA signaling as GEFs, we postulated that p190RhoGAP, which was reported to alter its substrate specificity from RhoA to Rac1 under certain conditions [39, 41, 46], is part of a putative complex and might be responsible for the observed changes in the presence of RGS3L. We, therefore, performed reciprocal co-immunoprecipitation experiments in NRCM transduced

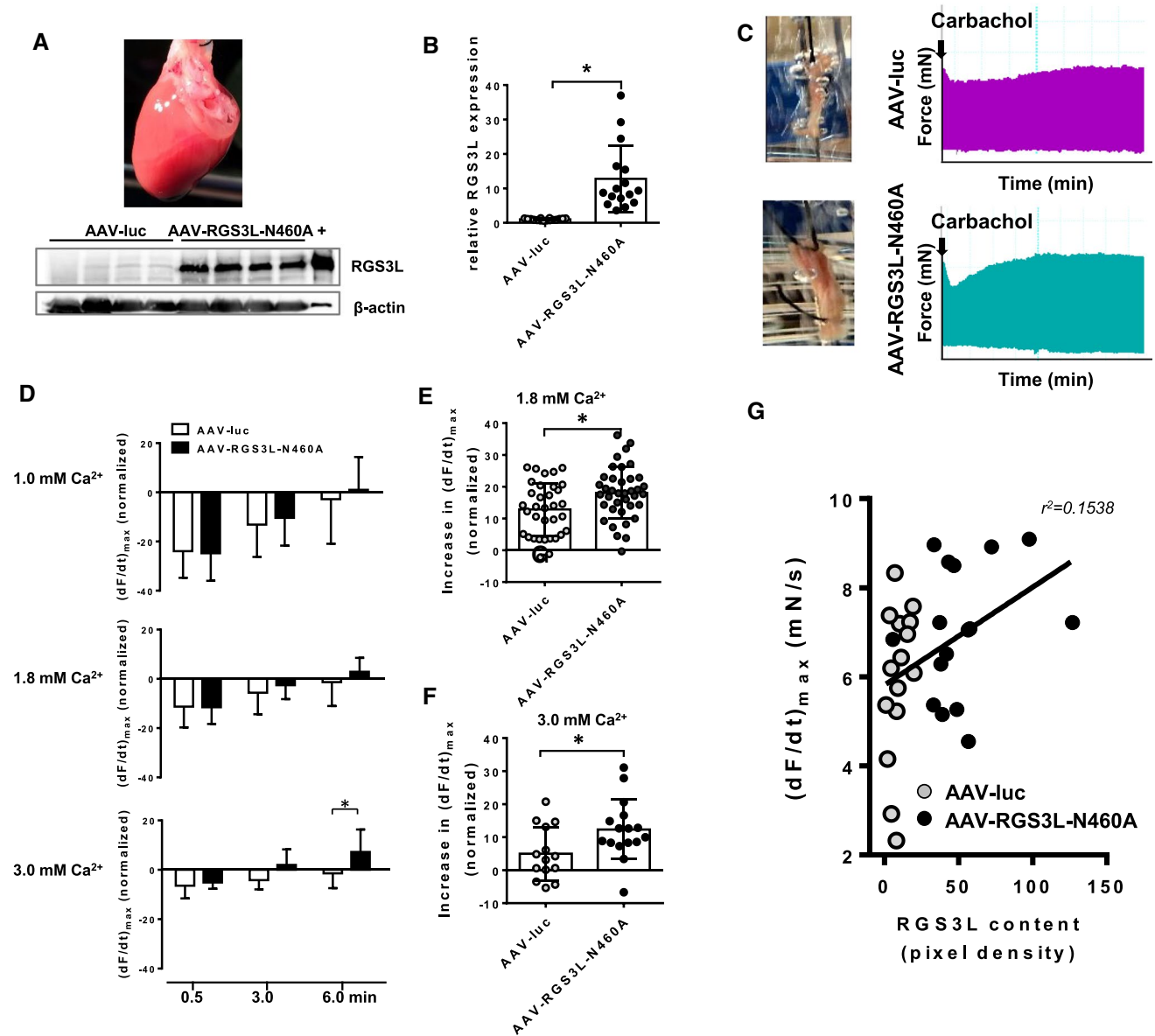


**Fig. 4** Effect of RGS3L–N460A expression on contractility of rat ventricular muscle strips. **A, B** RGS3L-Expression in rat ventricular muscle strips. Male Wistar rats were injected either with an AAV9–CMV–MLC1500-virus encoding RGS3L–N460A or AAV9–ssCMV–MLC1500-luc control virus. The expression of RGS3L in the muscle strips was analyzed after 2 months. A representative blot (**A**) and quantification (**B**) of the relative amount of RGS3L protein compared to the control are shown of  $n=16/16$  muscle strips from 4/4 animals, values are mean + SD,  $*p < 0.0001$ , +, lysate of NRCM overexpressing RGS3-N460A. **C** Representative recordings of the inotropic effects of carbachol (100  $\mu$ M) observed in control transduced and muscle strips overexpressing RGS3L–N460A measured in a Radnoti organ bath System (ADInstrument). **D** Time course (1.5 min, 3 min, 6 min) showing the development of the carbachol-

induced inotropic response at different  $Ca^{2+}$ -concentrations (1 mM, 1.8 mM, 3 mM). Data are shown as the percentage change of  $(dF/dt)_{max}$  relative to basal. Values are mean of  $n=14-29$  muscle strips from 4 to 8 animals + SD,  $*p < 0.01$ . **E** Relative increase in the maximal development of force ( $(dF/dt)_{max}$ ) analyzed between the 0.5 and 6 min timepoints measured in a buffer containing 1.8 mM  $Ca^{2+}$ . Values are mean of  $n=34/38$  muscle strips from 7/8 animals + SD,  $*p < 0.01$ . **F** Relative increase in the maximal development of force ( $(dF/dt)_{max}$ ) analyzed between the 0.5 and 6 min timepoints measured in a buffer containing 3 mM  $Ca^{2+}$ . Values are mean of  $n=34/37$  muscle strips + SD,  $*p < 0.05$ . **G** Correlation of the maximal contractility  $(dF/dt)_{max}$  6 min after carbachol-stimulation and the RGS3L expression of the muscle strips normalized as percentage of a positive control. Values are means of  $n=16/15$  muscle strips from 4/4 animals

with the RGS3L–N460A encoding adenovirus. In line with our hypothesis, p190RhoGAP could be co-immunoprecipitated from NRCM lysates with an anti-RGS3 antibody.

Similarly, RGS3L–N460A was co-immunoprecipitated with the anti-p190RhoGAP antibody. Treatment of the NRCM with carbachol before cell lysis increased the amount of

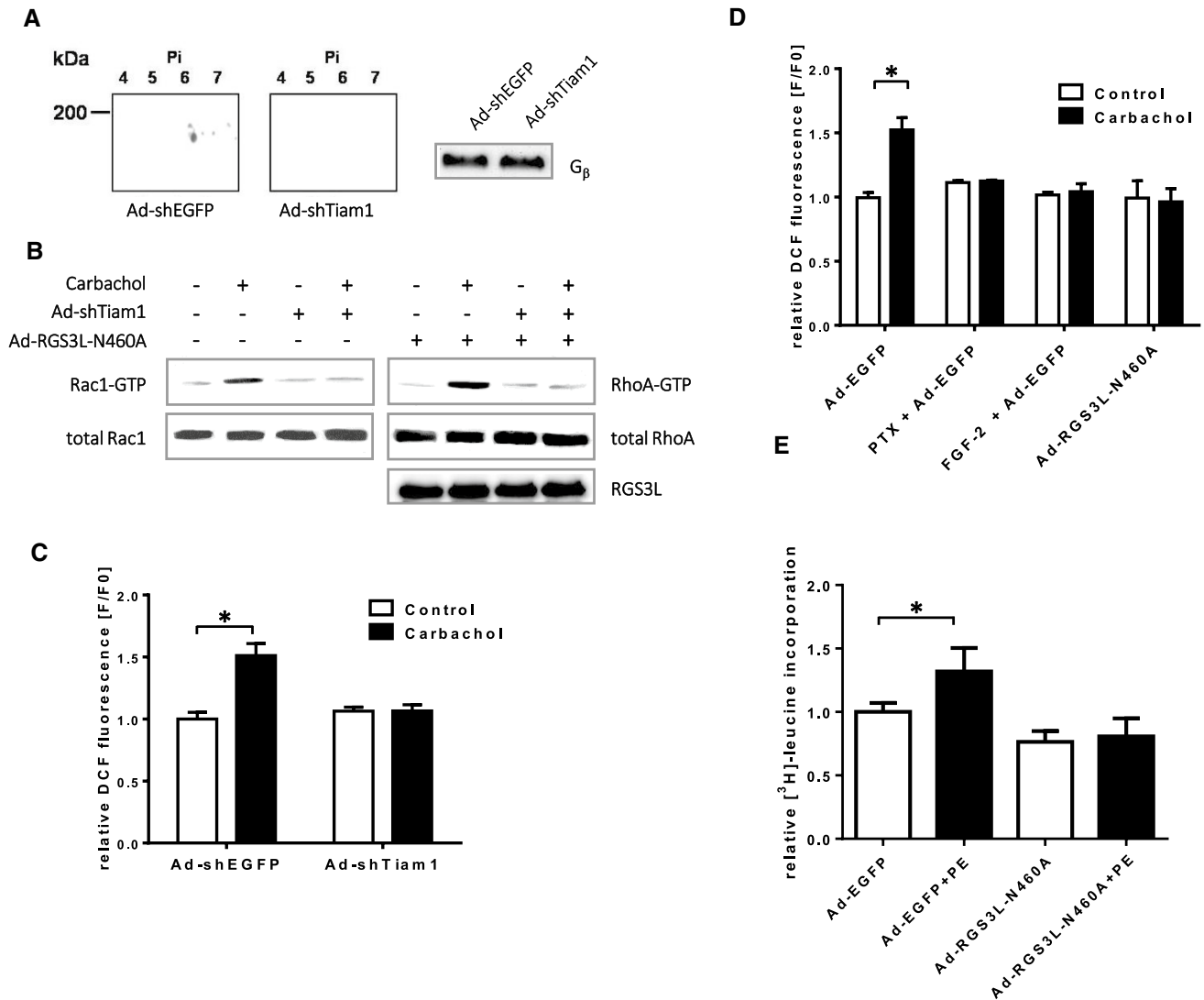


**Fig. 5** Effect of Tiam1-downregulation and RGS3L-N460A over-expression on carbachol-induced Rac1-activation and Rac1-effector functions NRCMs. Cells were transduced with or without Ad-shEGFP or Ad-shTiam1 for 72 h. **A** Tiam1 expression was monitored by 2D gel electrophoresis and immunoblot.  $G_{\beta}$  was used as a loading control. **B** Cells were transduced with Ad-shEGFP, Ad-shTiam1 and Ad-RGS3L-N460A for 72 h as indicated. Levels of RhoA-GTP and Rac1-GTP were determined after 5 min stimulation with or without carbachol. **C**, **D** Quantification of ROS-production in NRCMs by DCF fluorescence. **C** NRCMs were transduced with Ad-shEGFP or Ad-shTiam1 for 72 h. **D** Cells were transduced with Ad-EGFP or

Ad-RGS3L-N460A for 24 h and additionally treated with 100 ng/ml PTX or 50 ng/ml FGF2 for 24 h as indicated. Thereafter, the cells were stimulated with carbachol or solvent for 5 min at 37 °C. Values are mean + SD ( $n=6-10$ ),  $*p < 0.05$ . **E** Effect of the RGS3L-N460A-Expression on the Phenylephrine (PE) induced cellular hypertrophy. One  $\mu\text{Ci/ml}$  [ $^3\text{H}$ ]-leucine was added into the culture medium shortly after stimulation. After 24 h cellular protein was collected and [ $^3\text{H}$ ]-content was determined. Measurements were performed in 3 replicates. Values are mean + SD ( $n=3/6$  (EGFP/RGS3L-N460A),  $*p < 0.05$ )

the co-precipitated interaction partner by two-to-threefold (Fig. 6A–D). As a weak carbachol-induced RhoA activation also occurred in NRCM in a RGS3L sensitive manner (see Fig. 1E), we studied the p190RhoGAP/RGS3L interaction also in non-transduced NRCM. As these conditions are below the detection level of the co-immunoprecipitation assay, we performed a more sensitive proximity ligation assay (PLA) in NRCM. Thereby, we detected a complex

formation already under basal conditions. In accordance with the co-immunoprecipitation assays, carbachol significantly increased the interaction between both proteins, indicating that the carbachol-induced p190RhoGAP/RGS3L complex formation occurs also in native conditions (Fig. 6E, F).

The specificity of a GAP can be monitored by binding to constitutively active monomeric GTPases [58]. Therefore,

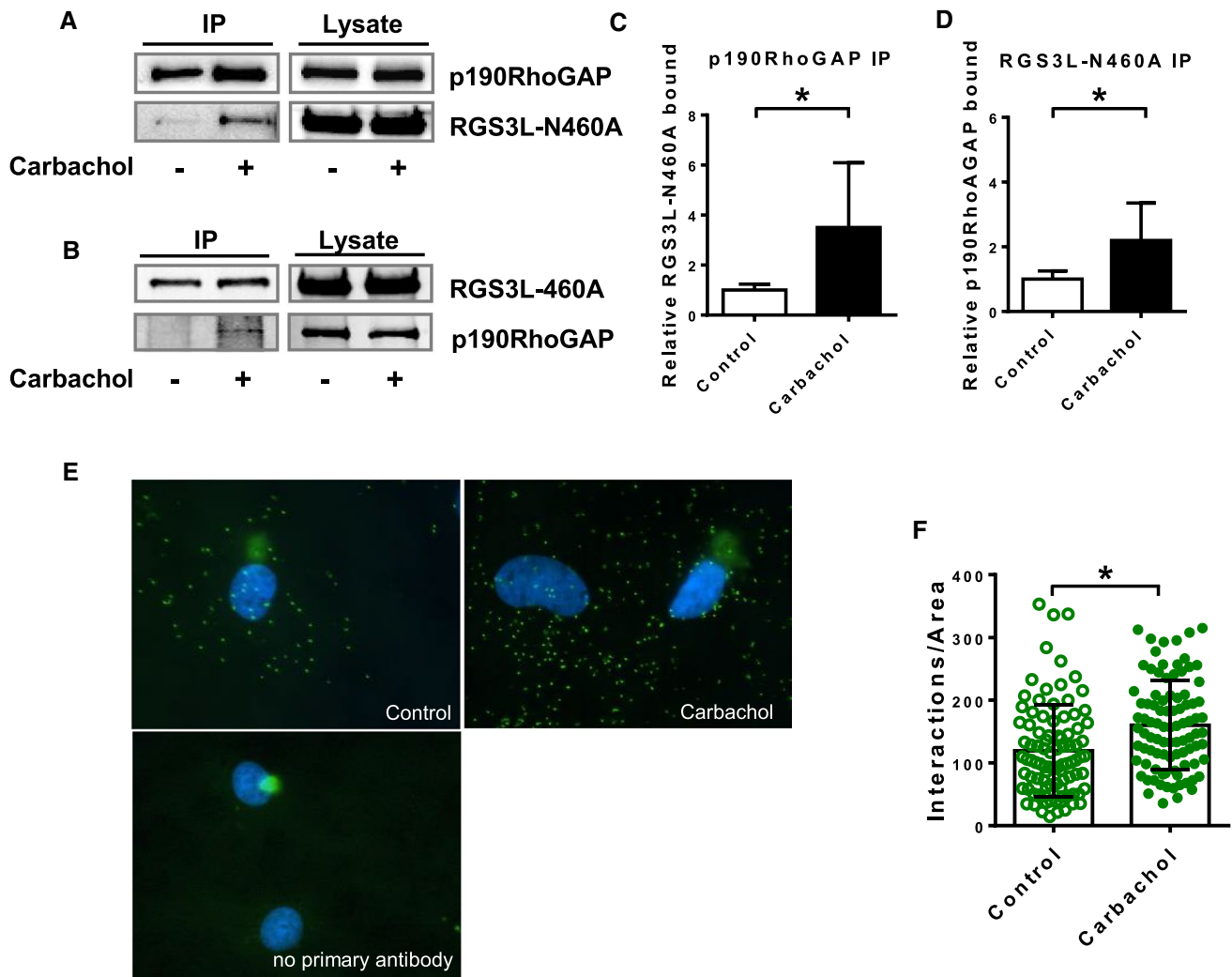


**Fig. 6** Visualization of the interaction of p190RhoGAP with RGS3L in NRCM. For co-immunoprecipitation experiments cells were transfected with the Ad-EGFP or Ad-RGS3L-N460A and 48 h later, cells were stimulated without and with carbachol for 5 min. Immunoprecipitations were performed using either anti-p190RhoGAP or anti-RGS3 antibodies. Western blots were probed with the corresponding secondary antibodies. Total amount of p190RhoGAP or RGS3L in the cell lysate was used as loading control. Representative experiments (**A**, **B**) and quantification of the relative amount of bound proteins compared to the non-stimulated control (**C**, **D**) are shown of

$n=11$  (**C**) or  $n=8$  (**D**) experiments. Values are mean + SD,  $*p < 0.05$ . **E** Visualization and quantification of the RGS3L-p190RhoGAP interaction using proximity ligation assay, NRCMs were plated on coverslips were stimulated without and with carbachol for 5 min. Phase contrast pictures, DAPI staining and proximity ligation (PLA) were performed. For negative control no primary antibodies were used **F** Quantification of the positive PLA-reactions. The number of the green fluorescent dots per cell was determined for 92 cells from three experiments. Values are mean + SD,  $*p < 0.05$

we studied whether RGS3L expression can alter the substrate specificity of overexpressed p190RhoGAP in HEK cells, the system in which the RGS3L-dependent switch from Rac1 to RhoA was originally characterized [87]. Co-transfection of RGS3L-N460A with p190RhoGAP reduced the binding of p190RhoGAP to the constitutively active RhoAQ63L mutant (Fig. 7A, B) and reciprocally increased the binding to the constitutively active Rac1Q61L mutant (Fig. 7C, D), supporting our hypothesis of a substrate switch of p190RhoGAP. Like the RGS3L-N460A mutant, wild-type RGS3L, but not the N-terminally truncated isoform

RGS3S is able to confer RhoA activation [87]. To test whether the switch in GAP activity of p190RhoGAP follows a similar pattern, we co-transfected HEK-293 cells with p190RhoGAP together with RGS3-N460A or RGS3S encoding constructs (Fig. 7E). In accordance with its ability to confer RhoA activation, the change in the GAP activity of p190RhoGAP was only observed in the presence of wild-type RGS3L and its N460A mutant, but not when RGS3S was expressed. This clearly demonstrates that the extended N-terminus of RGS3L is not only required for the  $G\beta\gamma$  binding [87], but is also a requisite for the regulation of

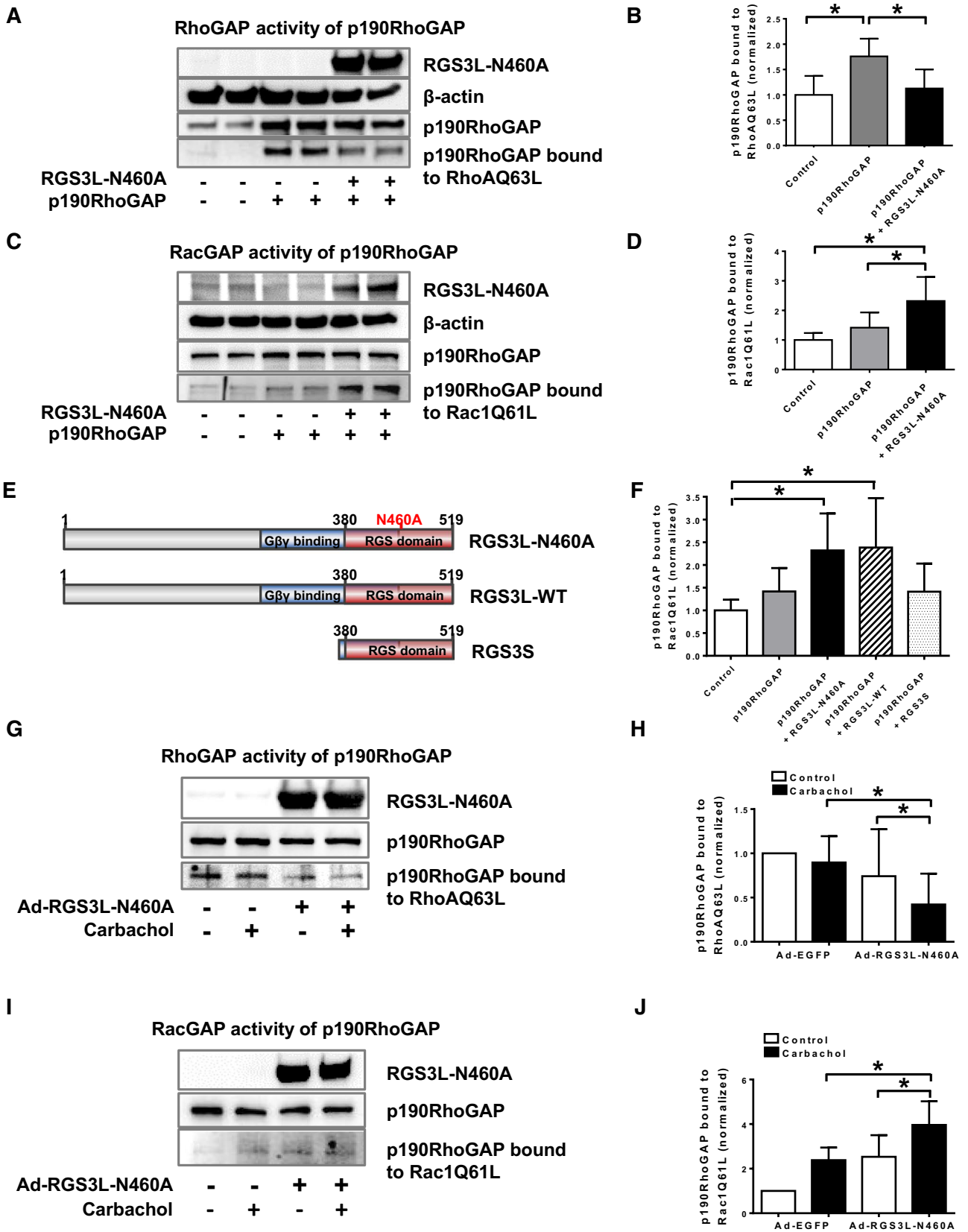


**Fig. 7** Measurement of the RhoAGAP and Rac1GAP activity of p190RhoGAP in HEK-293 cells and NRCM. **A–F** Measurement of the p190RhoGAP-activity in HEK-293 cells expressing p190RhoGAP with or without RGS3L. Functionally active p190RhoGAP was precipitated from the cell lysates with constitutive active RhoAQ63L–GST (**A, B**) or constitutive active Rac1Q61L–GST (**C, D**) coated beads. Immunostaining with anti-p190RhoGAP-antibody was used to detect p190RhoGAP in the precipitates (active p190RhoGAP) and in total lysates (loading control). Representative immunoblots of experiments performed in duplicate (**A, C**) as well as quantification of pixel density of  $n=5$  experiments (**B, D**) are shown. p190RhoGAP bound to RhoAQ63L or Rac1Q61L was normalized to the loading control. Values are mean + SD,  $*p < 0.05$ . **E** Molecular structure of the used RGS3 isoforms. **F** Measurement of the RacGAP activity of p190RhoGAP in HEK-293 cells expressing the indicated RGS3 isoforms. Values are mean + SD,  $n=5$ ,  $*p < 0.05$ . **G–J** Measurement of the RhoAGAP- and Rac1GAP-activity of p190RhoGAP in NRCM. After 48 h transduction with Ad-RGS3L-N460A or Ad-EGFP, cells were incubated with or without carbachol for 5 min. Relative RhoAGAP/Rac1GAP activity of p190RhoGAP was determined by the amount of bound p190RhoGAP to RhoAQ63L- or Rac1Q61L-coated beads normalized to the total amount of p190RhoGAP in cell lysates. Representative experiments (**G, I**) as well as quantification of the p190RhoGAP activities (**H, J**) are shown. The control value was set to 1.0 in each individual experiment. The other values are shown as mean + SD of  $n=9$  (**H**) or  $n=7$  (**J**) independent experiments. One-way ANOVA with Tukey's multiple comparison was performed for these values,  $*p < 0.05$

the GAP activity of p190RhoGAP (Fig. 7F). Next, we determined whether carbachol could change the substrate specificity of endogenously expressed p190RhoGAP for RhoA and Rac1 in the presence of RGS3L in NRCM. Without RGS3L–N460A expression, p190RhoGAP bound predominantly to constitutively active RhoA (Fig. 7G). In contrast, when RGS3L–N460A was expressed, carbachol reduced the binding of p190RhoGAP to RhoAQ63L and increased the binding to Rac1Q61L (Fig. 7G–J). The switch was detectable after 3 min and more prominent at 5 min (Supplemental Fig S2). Taken together these data clearly indicate that the interaction of RGS3L and p190RhoGAP is essential for re-balancing the activity of Rac1 and RhoA in response to carbachol in cardiomyocytes.

## Discussion

There is increasing evidence that cholinergic signaling could play a protective role in heart failure [36, 38] as the stimulation of the *nervus vagus* could protect the heart from remodeling and improved survival in animal heart failure models. However, whether such an approach is feasible in humans is a matter of debate. The first clinical trials investigating this promising therapeutic approach for human heart failure were not as beneficial as expected [44, 45, 60, 70]. During ischemia/reperfusion after myocardial infarction, however, vagal stimulation improved the outcome in a small cohort study [27, 93]. Nevertheless, muscarinic receptors play an

important role in the control of cardiac and vascular functions. The  $M_2R$  is the dominant cholinergic receptor subtype in the heart. However, surprisingly, it is also expressed in ventricular cardiomyocytes lacking parasympathetic innervation [14, 55].  $M_2Rs$  and  $G_i$  proteins are upregulated in heart failure [13, 84, 91] and exhibit a protective role in cardiac ventricular function and against the occurrence of cardiac arrhythmias [23, 37, 95]. On the other hand, chronic carbachol infusion sensitized the myocardium to cAMP-induced arrhythmia, most likely by reducing the content of PTX-sensitive  $G_i$  proteins in cardiomyocytes [18, 63]. Interestingly, it was recently shown that in addition to the parasympathetic regulation, acetylcholine (ACh) is secreted directly from cardiomyocytes [62, 66]. This non-neuronal ACh plays an important protective role in the regulation of myocardial function in both basal as well as in pathologic conditions and might be a possible therapeutic target in cardiovascular diseases [32, 38, 43, 52, 66, 69]. Cardiac ACh protected the heart from remodeling and mice lacking this non-neuronal source of ACh showed increased oxidative stress, remodeling, and hypertrophy [51, 65]. In addition, in heart failure a cholinergic trans-differentiation of the cardiac sympathetic nerves via cytokines secreted from the failing myocardium occurs [19, 33, 59], which might represent another source of ventricular ACh. Therefore, in addition to the correction of the sympathovagal balance in the heart, the so far not fully understood cholinergic signaling through  $M_2Rs$  in ventricular cardiomyocytes might be beneficial in the failing heart, possibly providing a new target for treatment of cardiovascular diseases [32].

Based on data obtained from a model of experimental heart failure in rats, which showed a ROCK-mediated inotropic response to  $M_2R$  activation only in failing hearts [30] and a RhoA/ROCK-mediated, carbachol-induced inotropy in neonatal rat hearts upon  $M_2R$  activation [40], we propose that the carbachol-induced RhoA/ROCK-mediated responses are elicited by this receptor subtype. This interpretation is supported by the sensitivity of the carbachol-induced RhoA activation to PTX treatment. In contrast to the  $G_{q/11}$ -mediated RhoA activation elicited by the  $M_3R$  [47], which might contribute to the regulation of cardiac contractility [35], the  $M_2R$ -induced,  $G_{i/o}$ -mediated RhoA activation in the presence of RGS3L is PTX sensitive [87]. We, therefore, studied the role of RGS3L in mediating a carbachol-induced RhoA activation in cardiomyocytes (NRCM, AMVM). We obtained evidence that the amount of expressed RGS3L regulates whether a carbachol-induced RhoA activation occurs or not. Whereas the depletion of RGS3L completely abolished the carbachol-induced RhoA activation, increasing its expression level, either by FGF2 treatment or adenoviral expression, strongly enhanced the ability of carbachol to activate RhoA. In accordance with the previously described pathway mediating the  $M_2R$ -induced

RhoA activation in HEK cells [87], the carbachol-induced RhoA activation in NRCM was inhibited by PTX and LY294002 treatment, indicating the involvement  $G_{i/o}$  proteins and the  $G\beta\gamma$ -dependent activation of PI3K (Fig. 8).

Similar to observations in the artificial  $M_2R$ -expressing HEK cell system, the increased carbachol-induced RhoA activation was accompanied by a decrease in carbachol-induced Rac1 activation.  $G_{i/o}$ -coupled GPCRs, including  $M_2Rs$ , are known to activate Rac1 in a variety of cell types [64]. In cardiomyocytes, the  $G_{i/o}$ -dependent Rac1 activation is mediated by  $G\beta\gamma$  dimers and involves the activation of PI3K and the Rac-GEF Tiam1 [85]. Rac1 activity has essential functions in the heart and is also involved in the development of cardiovascular diseases, e.g., it is involved in the hypertrophic response in cardiomyocytes [10, 68, 85]. Moreover, Rac1 is an essential co-factor of certain NADPH oxidases, which induce through increased oxidative stress cardiac dysfunction and injury [17, 48, 49, 57]. Thus, mice expressing constitutively active Rac1 developed cardiomyopathy and exhibited a post-ischemic contractile dysfunction [80, 81]. Therefore, inhibition of Rac1 signaling by enhanced RGS3L expression is a potential cardioprotective therapeutic strategy in cardiac hypertrophy, fibrosis,

arrhythmias, and heart failure [3, 20]. In line with this interpretation, upregulation or overexpression of RGS3L in NRCM suppressed the carbachol-induced ROS production, the phenylephrine-induced hypertrophic protein synthesis in NRCM, and hypertrophy induced by the inflammatory stimulus PGE2 [83]. In addition, the RGS3L upregulation likely interferes with the detrimental  $G\beta\gamma$ -mediated, muscarinic receptor induced activation of p38 mitogen-activated protein kinases, acting upstream of ROS production [28, 53, 73].

Interestingly, the signaling pathway used by  $M_2Rs$  to increase RhoA activity in the presence of RGS3L (see Fig. 8 and [87]) is similar or even identical to that used to activate Rac1 in the absence of RGS3L. This interpretation is supported by the data obtained by PTX treatment, PI3K inhibition, and Tiam1 depletion, which similarly abolished, both carbachol-induced RhoA and Rac1 activity observed with and without RGS3L–N460A expression, respectively. As mentioned before, Tiam1 does not induce an activation of other monomeric GTPases than Rac1 in living cells [21, 85]. Therefore, it is likely that the switch from Rac1 to RhoA activation in the presence of RGS3L is regulated by another molecule, most likely attracted to the same signaling complex by binding to  $G\beta\gamma$ /RGS3L. A potential candidate was p190RhoGAP as it is expressed in cardiomyocytes and most importantly can switch its substrate preference from RhoA to Rac1 [39, 41, 46]. In general, the regulation of the GAP activity can occur by several ways, such as autoregulation, lipid-binding, protein-binding, phosphorylation, or changing the subcellular localization [4, 16, 41, 46, 54, 74]. Moreover, by a recent meta-analysis, which aimed to evaluate sequence–structure–function relationship of different RhoGAPs and Rho proteins, it was suggested that the RhoGAP domain itself is rather nonselective and under cell-free conditions it can be even inefficient [2]. Instead, other domains of RhoGAPs can determinate the substrate specificity and fine-tune the catalytic efficiency of the GAP domain in the cell. In accordance with that notion, we obtained evidence that RGS3L is able to form a complex with p190RhoGAP and thereby its substrate preference switched from RhoA to Rac1. In line with this hypothesis, the downregulation of the endogenous RGS3L expression increased the basal activity of Rac1 (see Fig. 1G). Most importantly, the complex formation in cardiomyocytes is regulated by muscarinic receptors, thus likely accounting for the loss in carbachol-induced Rac1 activity and simultaneously increasing RhoA–GTP levels (Fig. 8). Taken together, our data demonstrate an interesting new mechanism involving an  $M_2R$ -induced switch which regulates the Rac1–RhoA balance in cardiomyocytes, and could account for the  $M_2R$ -induced increased cardiac contractility seen in experimental heart failure and neonatal rat hearts [30, 40]. In line with this hypothesis, we observed

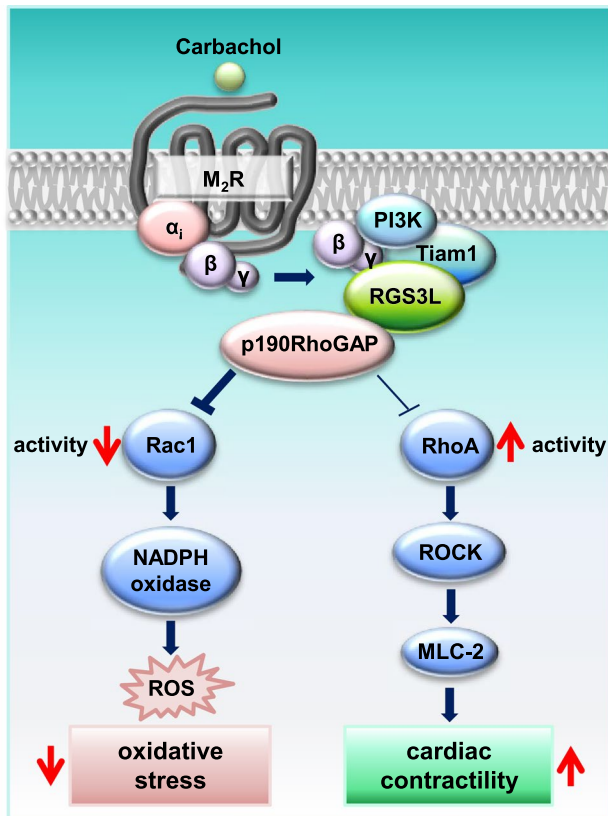


**Fig. 8** Schematic overview of the RGS3L-mediated switch in  $M_2R$  signaling from Rac1 to RhoA activation and its functional consequences in cardiomyocytes



an enhanced carbachol-induced phosphorylation of MLC-2 upon expression of RGS3L–N460A which was sensitive to ROCK inhibition.

The *ex vivo* contractility measurements of ventricular muscle strips from rats in which RGS3L–N460A was expressed by a cardiotropic AAV construct [6] revealed a positive correlation between the RGS3L–N460A expression level and an increase in contractility and allowed for carbachol-induced inotropy in a  $\text{Ca}^{2+}$ -dependent manner. This  $\text{Ca}^{2+}$ -dependency fits well to the effects known of increased RhoA and ROCK activation in cardiomyocytes, which allows for an increased phosphorylation of MLC through inhibition of MLC-phosphatase at higher  $\text{Ca}^{2+}$  concentrations within the cell [78].

As this muscarinic inotropic mechanism *bona fide* bypasses cAMP signaling it might be part of the beneficial effects of non-neuronal ACh in heart failure together with the afore discussed decrease in Rac1-dependent ROS production and cardiomyocyte hypertrophy. Therefore, it will be interesting to determine if there is therapeutic potential of AAV-mediated RGS3L–N460A expression in experimental heart failure models.

## Conclusions, study limitations and further perspectives

In this study we combined several *in vitro* models, NRCM, AMVCM, and HEK-293 cells, to clarify the mechanism how  $G_{i/o}$ -coupled muscarinic receptors, which are based on our previous work most likely of the  $M_2$  subtype ([30, 40, 87], can induce RhoA activation dependent on the expression of RGS3L. Our data demonstrate a  $G_{i/o}$ -dependent complex formation of RGS3L with p190RhoGAP, which likely depends on the known interaction of RGS3L with  $G\beta\gamma$  dimers [73, 87], that switches the GAP activity of p190RhoGAP from RhoA to Rac1. As a consequence, the agonist-induced Rac1 activity is decreased, whereas the RhoA activity is increased.

NRCM and AMVCM are from different species and largely differ regarding their differentiation, compartmentalization, and fetal vs. mature gene expression. HEK-293 cells are even regarded as an artificial cellular model. Thus, the finding that the  $G_{i/o}$ /RGS3L dependent signaling can be observed in different species and developmental stages indicate a rather common signaling pathway, which generally regulates the activation of RhoGTPases, e.g., by  $M_2$ Rs, dependent on the expression level of RGS3L in cardiomyocytes and is already present in early developmental stages. In line with this interpretation an increase in RhoA activity caused by carbachol stimulation was, as far as studied, always accompanied by a reduction in Rac1 activation.

The  $M_2$ R-induced, RhoA/ROCK-mediated increase in cardiac contractility was first described in left ventricular

strips isolated from adult rat hearts developing heart failure after myocardial infarction [30]. To test the hypothesis, that the RGS3L expression level is crucial to carbachol induced inotropy, we choose a model in which a cardiomyocyte specific RGS3L overexpression can be achieved *in vivo* and the effect of this overexpression could be studied under similar experimental conditions as described before [30]. Although, an RGS3L-dependent, carbachol-induced increase in contractility could be demonstrated, this model has limitations in its significance. For example, it cannot predict whether RGS3L overexpression has a realistic chance to be developed into a therapeutic intervention for the treatment of heart failure. To study this, the RGS3L overexpression strategy has to be tested for example in mouse or rat heart failure models and analyzed *in vivo*, e.g., by echocardiography to assess its influence on cardiac contractility. In addition, the second likely beneficial effect of the RGS3L overexpression, the inhibition of the detrimental activation of Rac1-dependent signaling, which herein was only preliminary characterized in NRCM, can be analyzed in such models in more detail. We are, therefore, pursuing such a strategy in our laboratory.

**Supplementary Information** The online version contains supplementary material available at <https://doi.org/10.1007/s00395-022-00915-w>.

**Acknowledgements** This work was supported by a grant of the DZHK (German Centre for Cardiovascular Research) to T. W. S. L. was supported by a grant of Deutsche Forschungsgemeinschaft, SFB 1002, C02.

**Funding** Open Access funding enabled and organized by Projekt DEAL. DZHK (German Centre for Cardiovascular Research); Deutsche Forschungsgemeinschaft.

## Declarations

**Conflict of interest** The authors declare that they have no conflict of interest.

**Ethics approval** All animal experiments were performed in accordance to guidelines of the local animal ethics committee.

**Open Access** This article is licensed under a Creative Commons Attribution 4.0 International License, which permits use, sharing, adaptation, distribution and reproduction in any medium or format, as long as you give appropriate credit to the original author(s) and the source, provide a link to the Creative Commons licence, and indicate if changes were made. The images or other third party material in this article are included in the article's Creative Commons licence, unless indicated otherwise in a credit line to the material. If material is not included in the article's Creative Commons licence and your intended use is not permitted by statutory regulation or exceeds the permitted use, you will need to obtain permission directly from the copyright holder. To view a copy of this licence, visit <http://creativecommons.org/licenses/by/4.0/>.

## References

- Akki A, Zhang M, Murdoch C, Brewer A, Shah AM (2009) NADPH oxidase signaling and cardiac myocyte function. *J Mol Cell Cardiol* 47:15–22. <https://doi.org/10.1016/j.yjmcc.2009.04.004>
- Amin E, Jaiswal M, Derewenda U, Reis K, Nouri K, Koessmeier KT, Aspenstrom P, Somlyo AV, Dvorsky R, Ahmadian MR (2016) Deciphering the molecular and functional basis of RhoGAP family proteins: a systematic approach towards selective inactivation of Rho family proteins. *J Biol Chem* 291:20353–20371. <https://doi.org/10.1074/jbc.M116.736967>
- An LP, An SK, Wei XH, Fu SY, Wu HA (2015) Atorvastatin improves cardiac function of rats with chronic cardiac failure via inhibiting Rac1/P47phox/P67phox-mediated ROS release. *Eur Rev Med Pharmacol Sci* 19:3940–3946
- Bao H, Li F, Wang C, Wang N, Jiang Y, Tang Y, Wu J, Shi Y (2016) Structural Basis for the Specific Recognition of RhoA by the Dual GTPase-activating Protein ARAP3. *J Biol Chem* 291:16709–16719. <https://doi.org/10.1074/jbc.M116.736140>
- Barberis D, Casazza A, Sordella R, Corso S, Artigiani S, Settleman J, Comoglio PM, Tamagnone L (2005) p190 Rho-GTPase activating protein associates with plexins and it is required for semaphorin signalling. *J Cell Sci* 118:4689–4700. <https://doi.org/10.1242/jcs.02590>
- Bish LT, Sweeney HL, Muller OJ, Bekeredjian R (2011) Adeno-associated virus vector delivery to the heart. *Methods Mol Biol* 807:219–237. [https://doi.org/10.1007/978-1-61779-370-7\\_9](https://doi.org/10.1007/978-1-61779-370-7_9)
- Boissier P, Huynh-Do U (2014) The guanine nucleotide exchange factor Tiam1: a Janus-faced molecule in cellular signaling. *Cell Signal* 26:483–491. <https://doi.org/10.1016/j.cellsig.2013.11.034>
- Borner S, Schwede F, Schlipp A, Berisha F, Calebiro D, Lohse MJ, Nikolaev VO (2011) FRET measurements of intracellular cAMP concentrations and cAMP analog permeability in intact cells. *Nat Protoc* 6:427–438. <https://doi.org/10.1038/nprot.2010.198>
- Brodde OE, Michel MC (1999) Adrenergic and muscarinic receptors in the human heart. *Pharmacol Rev* 51:651–690
- Brown JH, Del Re DP, Sussman MA (2006) The Rac and Rho hall of fame: a decade of hypertrophic signaling hits. *Circ Res* 98:730–742. <https://doi.org/10.1161/01.RES.0000216039.75913.9e>
- Clerk A, Pham FH, Fuller SJ, Sahai E, Aktories K, Marais R, Marshall C, Sugden PH (2001) Regulation of mitogen-activated protein kinases in cardiac myocytes through the small G protein Rac1. *Mol Cell Biol* 21:1173–1184. <https://doi.org/10.1128/MCB.21.4.1173-1184.2001>
- Cuello F, Bardswell SC, Haworth RS, Yin X, Lutz S, Wieland T, Mayr M, Kentish JC, Avkiran M (2007) Protein kinase D selectively targets cardiac troponin I and regulates myofilament Ca<sup>2+</sup> sensitivity in ventricular myocytes. *Circ Res* 100:864–873. <https://doi.org/10.1161/01.RES.0000260809.15393.fa>
- DeMazumder D, Kass DA, O'Rourke B, Tomaselli GF (2015) Cardiac resynchronization therapy restores sympathovagal balance in the failing heart by differential remodeling of cholinergic signaling. *Circ Res* 116:1691–1699. <https://doi.org/10.1161/CIRCRESAHA.116.305268>
- Dhein S, van Koppen CJ, Brodde OE (2001) Muscarinic receptors in the mammalian heart. *Pharmacol Res* 44:161–182. <https://doi.org/10.1006/phrs.2001.0835>
- Dykxhoorn DM, Novina CD, Sharp PA (2003) Killing the messenger: short RNAs that silence gene expression. *Nat Rev Mol Cell Biol* 4:457–467. <https://doi.org/10.1038/nrm1129>
- Eberth A, Lundmark R, Gremer L, Dvorsky R, Koessmeier KT, McMahon HT, Ahmadian MR (2009) A BAR domain-mediated autoinhibitory mechanism for RhoGAPs of the GRAF family. *Biochem J* 417:371–377. <https://doi.org/10.1042/BJ20081535>
- Elnakish MT, Hassanain HH, Janssen PM, Angelos MG, Khan M (2013) Emerging role of oxidative stress in metabolic syndrome and cardiovascular diseases: important role of Rac/NADPH oxidase. *J Pathol* 231:290–300. <https://doi.org/10.1002/path.4255>
- Eschenhagen T, Mende U, Diederich M, Hertle B, Memmesheimer C, Pohl A, Schmitz W, Scholz H, Steinfath M, Bohm M, Michel MC, Brodde OE, Raap A (1996) Chronic treatment with carbachol sensitizes the myocardium to cAMP-induced arrhythmia. *Circulation* 93:763–771. <https://doi.org/10.1161/01.cir.93.4.763>
- Fernandez SF, Canty JM Jr (2015) Adrenergic and cholinergic plasticity in heart failure. *Circ Res* 116:1639–1642. <https://doi.org/10.1161/CIRCRESAHA.115.306439>
- Ferri N, Corsini A, Bottino P, Clerici F, Contini A (2009) Virtual screening approach for the identification of new Rac1 inhibitors. *J Med Chem* 52:4087–4090. <https://doi.org/10.1021/jm8015987>
- Fleming IN, Batty IH, Prescott AR, Gray A, Kular GS, Stewart H, Downes CP (2004) Inositol phospholipids regulate the guanine-nucleotide-exchange factor Tiam1 by facilitating its binding to the plasma membrane and regulating GDP/GTP exchange on Rac1. *Biochem J* 382:857–865. <https://doi.org/10.1042/BJ20040916>
- Gomez J, Shannon H, Kostenis E, Felder C, Zhang L, Brodtkin J, Grinberg A, Sheng H, Wess J (1999) Pronounced pharmacologic deficits in M2 muscarinic acetylcholine receptor knockout mice. *Proc Natl Acad Sci USA* 96:1692–1697. <https://doi.org/10.1073/pnas.96.4.1692>
- Grimm M, Gsell S, Mittmann C, Nose M, Scholz H, Weil J, Eschenhagen T (1998) Inactivation of (G $\alpha$ ) proteins increases arrhythmogenic effects of beta-adrenergic stimulation in the heart. *J Mol Cell Cardiol* 30:1917–1928. <https://doi.org/10.1006/jmcc.1998.0769>
- Hansen A, Eder A, Bonstrup M, Flato M, Mewe M, Schaaf S, Aksehirlioglu B, Schworer A, Uebeler J, Eschenhagen T (2010) Development of a drug screening platform based on engineered heart tissue. *Circ Res* 107:35–U70. <https://doi.org/10.1161/Circresaha.109.211458>
- Harvey RD, Belevych AE (2003) Muscarinic regulation of cardiac ion channels. *Br J Pharmacol* 139:1074–1084. <https://doi.org/10.1038/sj.bjp.0705338>
- Herbrand U, Ahmadian MR (2006) p190-RhoGAP as an integral component of the Tiam1/Rac1-induced downregulation of Rho. *Biol Chem* 387:311–317. <https://doi.org/10.1515/BC.2006.041>
- Heusch G (2017) Vagal cardioprotection in reperfused acute myocardial infarction. *JACC Cardiovasc Interv* 10:1521–1522. <https://doi.org/10.1016/j.jcin.2017.05.063>
- Heusch P, Canton M, Aker S, van de Sand A, Konietzka I, Rassaf T, Menazza S, Brodde OE, Di Lisa F, Heusch G, Schulz R (2010) The contribution of reactive oxygen species and p38 mitogen-activated protein kinase to myofilament oxidation and progression of heart failure in rabbits. *Br J Pharmacol* 160:1408–1416. <https://doi.org/10.1111/j.1476-5381.2010.00793.x>
- Hori M, Okamoto H (2012) Heart rate as a target of treatment of chronic heart failure. *J Cardiol* 60:86–90. <https://doi.org/10.1016/j.jicc.2012.06.013>
- Hussain RI, Qvigstad E, Birkeland JA, Eikemo H, Glende A, Sjaastad I, Skomedal T, Osnes JB, Levy FO, Krobert KA (2009) Activation of muscarinic receptors elicits inotropic responses in ventricular muscle from rats with heart failure through myosin light chain phosphorylation. *Br J Pharmacol* 156:575–586. <https://doi.org/10.1111/j.1476-5381.2009.00016.x>
- Jungmann A, Leuchs B, Rommelaere J, Katus HA, Muller OJ (2017) Protocol for efficient generation and characterization of adeno-associated viral vectors. *Hum Gene Ther Methods* 28:235–246. <https://doi.org/10.1089/hgtb.2017.192>

32. Kakinuma Y (2015) Future perspectives of a cardiac non-neuronal acetylcholine system targeting cardiovascular diseases as an adjunctive tool for metabolic intervention. *Int Immunopharmacol* 29:185–188. <https://doi.org/10.1016/j.intimp.2015.05.029>
33. Kanazawa H, Ieda M, Kimura K, Arai T, Kawaguchi-Manabe H, Matsuhashi T, Endo J, Sano M, Kawakami T, Kimura T, Monkawa T, Hayashi M, Iwanami A, Okano H, Okada Y, Ishibashi-Ueda H, Ogawa S, Fukuda K (2010) Heart failure causes cholinergic transdifferentiation of cardiac sympathetic nerves via gp130-signaling cytokines in rodents. *J Clin Invest* 120:408–421. <https://doi.org/10.1172/JCI39778>
34. Kishi T (2016) Deep and future insights into neuromodulation therapies for heart failure. *J Cardiol* 68:368–372. <https://doi.org/10.1016/j.jicc.2016.05.010>
35. Kitazawa T, Asakawa K, Nakamura T, Teraoka H, Unno T, Komori S, Yamada M, Wess J (2009) M3 muscarinic receptors mediate positive inotropic responses in mouse atria: a study with muscarinic receptor knockout mice. *J Pharmacol Exp Ther* 330:487–493. <https://doi.org/10.1124/jpet.109.153304>
36. La Rovere MT, Bigger JT Jr, Marcus FI, Mortara A, Schwartz PJ (1998) Baroreflex sensitivity and heart-rate variability in prediction of total cardiac mortality after myocardial infarction. ATRAMI (Autonomic Tone and Reflexes After Myocardial Infarction) Investigators. *Lancet* 351:478–484. [https://doi.org/10.1016/s0140-6736\(97\)11144-8](https://doi.org/10.1016/s0140-6736(97)11144-8)
37. LaCroix C, Freeling J, Giles A, Wess J, Li YF (2008) Deficiency of M2 muscarinic acetylcholine receptors increases susceptibility of ventricular function to chronic adrenergic stress. *Am J Physiol Heart Circ Physiol* 294:H810–820. <https://doi.org/10.1152/ajpheart.00724.2007>
38. Lara A, Damasceno DD, Pires R, Gros R, Gomes ER, Gavioli M, Lima RF, Guimaraes D, Lima P, Bueno CR Jr, Vasconcelos A, Roman-Campos D, Menezes CA, Sirvente RA, Salemi VM, Mady C, Caron MG, Ferreira AJ, Brum PC, Resende RR, Cruz JS, Gomez MV, Prado VF, de Almeida AP, Prado MA, Guatimosim S (2010) Dysautonomia due to reduced cholinergic neurotransmission causes cardiac remodeling and heart failure. *Mol Cell Biol* 30:1746–1756. <https://doi.org/10.1128/MCB.00996-09>
39. Levay M, Bartos B, Ligeti E (2013) p190RhoGAP has cellular RacGAP activity regulated by a polybasic region. *Cell Signal* 25:1388–1394. <https://doi.org/10.1016/j.cellsig.2013.03.004>
40. Levay M, Krobert KA, Wittig K, Voigt N, Bermudez M, Wolber G, Dobrev D, Levy FO, Wieland T (2013) NSC23766, a widely used inhibitor of Rac1 activation, additionally acts as a competitive antagonist at muscarinic acetylcholine receptors. *J Pharmacol Exp Ther* 347:69–79. <https://doi.org/10.1124/jpet.113.207266>
41. Levay M, Settleman J, Ligeti E (2009) Regulation of the substrate preference of p190RhoGAP by protein kinase C-mediated phosphorylation of a phospholipid binding site. *Biochemistry* 48:8615–8623. <https://doi.org/10.1021/bi900667y>
42. Levy MN (1971) Sympathetic-Parasympathetic Interactions in Heart. *Circ Res* 29:437–445. <https://doi.org/10.1161/01.Res.29.5.437>
43. Lewartowski B, Mackiewicz U (2015) The non-neuronal heart's acetylcholine in health and disease. *J Physiol Pharmacol* 66:773–778
44. Li M, Zheng C, Sato T, Kawada T, Sugimachi M, Sunagawa K (2004) Vagal nerve stimulation markedly improves long-term survival after chronic heart failure in rats. *Circulation* 109:120–124. <https://doi.org/10.1161/01.CIR.0000105721.71640.DA>
45. Li Y, Xuan YH, Liu SS, Dong J, Luo JY, Sun ZJ (2015) Short-term vagal nerve stimulation improves left ventricular function following chronic heart failure in rats. *Mol Med Rep* 12:1709–1716. <https://doi.org/10.3892/mmr.2015.3597>
46. Ligeti E, Dagher MC, Hernandez SE, Koleske AJ, Settleman J (2004) Phospholipids can switch the GTPase substrate preference of a GTPase-activating protein. *J Biol Chem* 279:5055–5058. <https://doi.org/10.1074/jbc.C300547200>
47. Lutz S, Freichel-Blomquist A, Yang Y, Rumenapp U, Jakobs KH, Schmidt M, Wieland T (2005) The guanine nucleotide exchange factor p63RhoGEF, a specific link between Gq/11-coupled receptor signaling and RhoA. *J Biol Chem* 280:11134–11139. <https://doi.org/10.1074/jbc.M411322200>
48. Ma J, Wang Y, Zheng D, Wei M, Xu H, Peng T (2012) Rac1 signalling mediates doxorubicin-induced cardiotoxicity through both reactive oxygen species-dependent and -independent pathways. *Cardiovasc Res* 97:77–87. <https://doi.org/10.1093/cvr/cvs309>
49. Maack C, Kartes T, Kilter H, Schafers HJ, Nickenig G, Bohm M, Laufs U (2003) Oxygen free radical release in human failing myocardium is associated with increased activity of rac1-GTPase and represents a target for statin treatment. *Circulation* 108:1567–1574. <https://doi.org/10.1161/01.CIR.0000091084.46500.BB>
50. Mertens AE, Roovers RC, Collard JG (2003) Regulation of Tiam1-Rac signalling. *FEBS Lett* 546:11–16. [https://doi.org/10.1016/s0014-5793\(03\)00435-6](https://doi.org/10.1016/s0014-5793(03)00435-6)
51. Miao Y, Bi XY, Zhao M, Jiang HK, Liu JJ, Li DL, Yu XJ, Yang YH, Huang N, Zang WJ (2015) Acetylcholine inhibits tumor necrosis factor alpha activated endoplasmic reticulum apoptotic pathway via EGFR-PI3K signaling in cardiomyocytes. *J Cell Physiol* 230:767–774. <https://doi.org/10.1002/jcp.24800>
52. Miao Y, Zhou J, Zhao M, Liu J, Sun L, Yu X, He X, Pan X, Zang W (2013) Acetylcholine attenuates hypoxia/reoxygenation-induced mitochondrial and cytosolic ROS formation in H9c2 cells via M2 acetylcholine receptor. *Cell Physiol Biochem* 31:189–198. <https://doi.org/10.1159/000343360>
53. Michel MC, Li Y, Heusch G (2001) Mitogen-activated protein kinases in the heart. *Naunyn Schmiedebergs Arch Pharmacol* 363:245–266. <https://doi.org/10.1007/s002100000363>
54. Minoshima Y, Kawashima T, Hirose K, Tonzuka Y, Kawajiri A, Bao YC, Deng X, Tatsuka M, Narumiya S, May WS Jr, Nosaka T, Semba K, Inoue T, Satoh T, Inagaki M, Kitamura T (2003) Phosphorylation by aurora B converts MgcRacGAP to a RhoGAP during cytokinesis. *Dev Cell* 4:549–560. [https://doi.org/10.1016/s1534-5807\(03\)00089-3](https://doi.org/10.1016/s1534-5807(03)00089-3)
55. Mittmann C, Pinkepank G, Stamatelopoulou S, Wieland T, Nurnberg B, Hirt S, Eschenhagen T (2003) Differential coupling of m-cholinoceptors to Gi/Go-proteins in failing human myocardium. *J Mol Cell Cardiol* 35:1241–1249. [https://doi.org/10.1016/s0022-2828\(03\)00235-9](https://doi.org/10.1016/s0022-2828(03)00235-9)
56. Mittmann C, Schuler C, Chung CH, Hoppner G, Nose M, Kehrl JH, Wieland T (2001) Evidence for a short form of RGS3 preferentially expressed in the human heart. *Naunyn Schmiedebergs Arch Pharmacol* 363:456–463. <https://doi.org/10.1007/s002100000376>
57. Nagase M, Ayuzawa N, Kawarazaki W, Ishizawa K, Ueda K, Yoshida S, Fujita T (2012) Oxidative stress causes mineralocorticoid receptor activation in rat cardiomyocytes: role of small GTPase Rac1. *Hypertension* 59:500–506. <https://doi.org/10.1161/HYPERTENSIONAHA.111.185520>
58. Noren NK, Arthur WT, Burridge K (2003) Cadherin engagement inhibits RhoA via p190RhoGAP. *J Biol Chem* 278:13615–13618. <https://doi.org/10.1074/jbc.C200657200>
59. Olivás A, Gardner RT, Wang L, Ripplinger CM, Woodward WR, Habecker BA (2016) Myocardial infarction causes transient cholinergic transdifferentiation of cardiac sympathetic nerves via gp130. *J Neurosci* 36:479–488. <https://doi.org/10.1523/JNEUROSCI.3556-15.2016>
60. Olshansky B (2016) Electrical Stimulation of the Vagus Nerve for Chronic Heart Failure: Is It Time to Pull the Plug? *J Card Fail* 22:643–645. <https://doi.org/10.1016/j.cardfail.2016.05.005>
61. Owen VJ, Burton PB, Mullen AJ, Birks EJ, Barton P, Yacoub MH (2001) Expression of RGS3, RGS4 and Gi alpha 2 in

- acutely failing donor hearts and end-stage heart failure. *Eur Heart J* 22:1015–1020. <https://doi.org/10.1053/euhj.2000.2578>
62. Rana OR, Schauerte P, Kluttig R, Schroder JW, Koenen RR, Weber C, Nolte KW, Weis J, Hoffmann R, Marx N, Saygili E (2010) Acetylcholine as an age-dependent non-neuronal source in the heart. *Auton Neurosci* 156:82–89. <https://doi.org/10.1016/j.autneu.2010.04.011>
  63. Reithmann C, Werdan K (1995) Chronic muscarinic cholinergic stimulation increases adenylyl cyclase responsiveness in rat cardiomyocytes by a decrease in the level of inhibitory G-protein alpha-subunits. *Naunyn Schmiedebergs Arch Pharmacol* 351:27–34. <https://doi.org/10.1007/BF00169060>
  64. Rossman KL, Der CJ, Sondel J (2005) GEF means go: turning on RHO GTPases with guanine nucleotide-exchange factors. *Nat Rev Mol Cell Biol* 6:167–180. <https://doi.org/10.1038/nrm1587>
  65. Roy A, Dakroub M, Tezini GC, Liu Y, Guatimosim S, Feng Q, Salgado HC, Prado VF, Prado MA, Gros R (2015) Cardiac acetylcholine inhibits ventricular remodeling and dysfunction under pathologic conditions. *FASEB J* 30:688–701. <https://doi.org/10.1096/fj.15-277046>
  66. Roy A, Fields WC, Rocha-Resende C, Resende RR, Guatimosim S, Prado VF, Gros R, Prado MA (2013) Cardiomyocyte-secreted acetylcholine is required for maintenance of homeostasis in the heart. *FASEB J* 27:5072–5082. <https://doi.org/10.1096/fj.13-238279>
  67. Salazar NC, Chen J, Rockman HA (2007) Cardiac GPCRs: GPCR signaling in healthy and failing hearts. *Biochim Biophys Acta* 1768:1006–1018. <https://doi.org/10.1016/j.bbamem.2007.02.010>
  68. Satoh M, Ogita H, Takeshita K, Mukai Y, Kwiatkowski DJ, Liao JK (2006) Requirement of Rac1 in the development of cardiac hypertrophy. *Proc Natl Acad Sci USA* 103:7432–7437. <https://doi.org/10.1073/pnas.0510444103>
  69. Saw EL, Kakinuma Y, Fronius M, Katara R (2018) The non-neuronal cholinergic system in the heart: a comprehensive review. *J Mol Cell Cardiol* 125:129–139. <https://doi.org/10.1016/j.yjmcc.2018.10.013>
  70. Schwartz PJ (2012) Vagal stimulation for the treatment of heart failure: a translational success story. *Heart* 98:1687–1689. <https://doi.org/10.1136/heartjnl-2012-302291>
  71. Settleman J, Albright CF, Foster LC, Weinberg RA (1992) Association between GTPase activators for Rho and Ras families. *Nature* 359:153–154. <https://doi.org/10.1038/359153a0>
  72. Settleman J, Narasimhan V, Foster LC, Weinberg RA (1992) Molecular cloning of cDNAs encoding the GAP-associated protein p190: implications for a signaling pathway from ras to the nucleus. *Cell* 69:539–549. [https://doi.org/10.1016/0092-8674\(92\)90454-k](https://doi.org/10.1016/0092-8674(92)90454-k)
  73. Shi CS, Lee SB, Sinnarajah S, Dessauer CW, Rhee SG, Kehrl JH (2001) Regulator of G-protein signaling 3 (RGS3) inhibits Gbetagamma 2-induced inositol phosphate production, mitogen-activated protein kinase activation, and Akt activation. *J Biol Chem* 276:24293–24300. <https://doi.org/10.1074/jbc.M100089200>
  74. Sirokmany G, Szidonya L, Kaldi K, Gaborik Z, Ligeti E, Geiszt M (2006) Sec14 homology domain targets p50RhoGAP to endosomes and provides a link between Rab and Rho GTPases. *J Biol Chem* 281:6096–6105. <https://doi.org/10.1074/jbc.M510619200>
  75. Sjaastad I, Schiander I, Sjetnan A, Qvigstad E, Bokenes J, Sandnes D, Osnes JB, Sejersted OM, Skomedal T (2003) Increased contribution of alpha 1- vs. beta-adrenoceptor-mediated inotropic response in rats with congestive heart failure. *Acta Physiol Scand* 177:449–458. <https://doi.org/10.1046/j.1365-201X.2003.01063.x>
  76. Skomedal T, Borthne K, Aass H, Geiran O, Osnes JB (1997) Comparison between alpha-1 adrenoceptor-mediated and beta adrenoceptor-mediated inotropic components elicited by norepinephrine in failing human ventricular muscle. *J Pharmacol Exp Ther* 280:721–729
  77. Skomedal T, Osnes JB, Oye I (1982) Differences between Alpha-Adrenergic and Beta-Adrenergic Inotropic Effects in Rat-Heart Papillary-Muscles. *Acta Pharmacol Toxicol* 50:1–12. <https://doi.org/10.1111/j.1600-0773.1982.tb00932.x>
  78. Somlyo AP, Somlyo AV (2003) Ca<sup>2+</sup> sensitivity of smooth muscle and nonmuscle myosin II: Modulated by G proteins, kinases, and myosin phosphatase. *Physiol Rev* 83:1325–1358. <https://doi.org/10.1152/physrev.00023.2003>
  79. Sonntag F, Kother K, Schmidt K, Weghofer M, Raupp C, Nieto K, Kuck A, Gerlach B, Bottcher B, Muller OJ, Lux K, Horer M, Kleinschmidt JA (2011) The assembly-activating protein promotes capsid assembly of different adeno-associated virus serotypes. *J Virol* 85:12686–12697. <https://doi.org/10.1128/JVI.05359-11>
  80. Sussman MA, Welch S, Walker A, Klevitsky R, Hewett TE, Price RL, Schaefer E, Yager K (2000) Altered focal adhesion regulation correlates with cardiomyopathy in mice expressing constitutively active rac1. *J Clin Invest* 105:875–886. <https://doi.org/10.1172/JCI8497>
  81. Talukder MA, Elnakish MT, Yang F, Nishijima Y, Alhaj MA, Velayutham M, Hassanain HH, Zweier JL (2012) Cardiomyocyte-specific Overexpression of an Active Form of Rac Predisposes the Heart to Increased Myocardial Stunning and Ischemia/Reperfusion Injury. *Am J Physiol Heart Circ Physiol* 304:H294–302. <https://doi.org/10.1152/ajpheart.00367.2012>
  82. Tilley DG (2011) G protein-dependent and G protein-independent signaling pathways and their impact on cardiac function. *Circ Res* 109:217–230. <https://doi.org/10.1161/CIRCRESAHA.110.231225>
  83. Toth AD, Schell R, Levay M, Vettel C, Theis P, Haslinger C, Alban F, Werhahn S, Frischbier L, Krebs-Haupenthal J, Thomas D, Grone HJ, Avkiran M, Katus HA, Wieland T, Backs J (2018) Inflammation leads through PGE/EP3 signaling to HDAC5/MEF2-dependent transcription in cardiac myocytes. *EMBO Mol Med* 10e:8536. <https://doi.org/10.15252/emmm.201708536>
  84. Vatner DE, Sato N, Galper JB, Vatner SF (1996) Physiological and biochemical evidence for coordinate increases in muscarinic receptors and Gi during pacing-induced heart failure. *Circulation* 94:102–107. <https://doi.org/10.1161/01.CIR.94.1.102>
  85. Vettel C, Wittig K, Vogt A, Wuertz CM, El-Armouche A, Lutz S, Wieland T (2012) A novel player in cellular hypertrophy: Gibetagamgamma/PI3K-dependent activation of the RacGEF TIAM-1 is required for alpha(1)-adrenoceptor induced hypertrophy in neonatal rat cardiomyocytes. *J Mol Cell Cardiol* 53:165–175. <https://doi.org/10.1016/j.yjmcc.2012.04.015>
  86. Vetter IR, Wittinghofer A (2001) The guanine nucleotide-binding switch in three dimensions. *Science* 294:1299–1304. <https://doi.org/10.1126/science.1062023>
  87. Vogt A, Lutz S, Rumenapp U, Han L, Jakobs KH, Schmidt M, Wieland T (2007) Regulator of G-protein signalling 3 redirects prototypical Gi-coupled receptors from Rac1 to RhoA activation. *Cell Signal* 19:1229–1237. <https://doi.org/10.1016/j.cellsig.2007.01.003>
  88. Wang H, Han H, Zhang L, Shi H, Schram G, Nattel S, Wang Z (2001) Expression of multiple subtypes of muscarinic receptors and cellular distribution in the human heart. *Mol Pharmacol* 59:1029–1036. <https://doi.org/10.1124/mol.59.5.1029>
  89. Wieland T, Lutz S, Chidiac P (2007) Regulators of G protein signalling: a spotlight on emerging functions in the cardiovascular system. *Curr Opin Pharmacol* 7:201–207. <https://doi.org/10.1016/j.coph.2006.11.007>
  90. Wildenberg GA, Dohn MR, Carnahan RH, Davis MA, Lobdell NA, Settleman J, Reynolds AB (2006) p120-catenin and p190RhoGAP regulate cell-cell adhesion by coordinating

- antagonism between Rac and Rho. *Cell* 127:1027–1039. <https://doi.org/10.1016/j.cell.2006.09.046>
91. Wilkinson M, Giles A, Armour JA, Cardinal R (1996) Ventricular, but not atrial, M2-muscarinic receptors increase in the canine pacing-overdrive model of heart failure. *Can J Cardiol* 12:71–76
  92. Will RD, Eden M, Just S, Hansen A, Eder A, Frank D, Kuhn C, Seeger TS, Oehl U, Wiemann S, Korn B, Koegl M, Rottbauer W, Eschenhagen T, Katus HA, Frey N (2010) Myomasp/LRRC39, a heart- and muscle-specific protein, is a novel component of the sarcomeric M-band and is involved in stretch sensing. *Circ Res* 107:1253–1264. <https://doi.org/10.1161/CIRCRESAHA.110.222372>
  93. Yu L, Huang B, Po SS, Tan T, Wang M, Zhou L, Meng G, Yuan S, Zhou X, Li X, Wang Z, Wang S, Jiang H (2017) Low-level tragus stimulation for the treatment of ischemia and reperfusion injury in patients with ST-segment elevation myocardial infarction: a proof-of-concept study. *JACC Cardiovasc Interv* 10:1511–1520. <https://doi.org/10.1016/j.jcin.2017.04.036>
  94. Zhang P, Mende U (2011) Regulators of G-protein signaling in the heart and their potential as therapeutic targets. *Circ Res* 109:320–333. <https://doi.org/10.1161/CIRCRESAHA.110.231423>
  95. Zhang S, He Z, Wang J, Wang L, Wu Y, Wang J, Lv T, Liu H (2015) Mitochondrial ultrastructural alterations and declined M2 receptor density were involved in cardiac dysfunction in rats after long term treatment with autoantibodies against M2 muscarinic receptor. *PLoS ONE* 10:e0129563. <https://doi.org/10.1371/journal.pone.0129563>
  96. Zhang S, Watson N, Zahner J, Rottman JN, Blumer KJ, Muslin AJ (1998) RGS3 and RGS4 are GTPase activating proteins in the heart. *J Mol Cell Cardiol* 30:269–276. <https://doi.org/10.1006/jmcc.1997.0591>